Journal of Medicinal Chemistry

Article

pubs.acs.org/jmc

Design and Synthesis of New Benzimidazole−Carbazole Conjugates for the Stabilization of Human Telomeric DNA, Telomerase Inhibition, and Their Selective Action on Cancer Cells

Basudeb Maji,[†] Krishan Kumar,[†] Mangesh Kaulage,[†,§] K. Muniyappa,[§] and Santanu Bhattacharya*[,†,‡]

[†]Department of Organic Chemistry, Indian Institute of Science, Bangalore, Karnataka 560 012, India

[‡]Jawaharlal Nehru Centre for Advanced Scientific Research, Bangalore, Karnataka 560 012, India

[§]Department of Biochemistry, Indian Institute of Science, Bangalore, Karnataka 560 012, India

Supporting Information

ABSTRACT: Cell-permeable small molecules that enhance the stability of the G-quadruplex (G4) DNA structures are currently among the most intensively pursued ligands for inhibition of the telomerase activity. Herein we report the design and syntheses of four novel benzimidazole−carbazole conjugates and demonstrate their high binding affinity to G4 DNA. S1 nuclease assay confirmed the ligand mediated G-quadruplex DNA protection. Additional evidence from Telomeric Repeat Amplification Protocol (TRAP-LIG) assay demonstrated efficient telomerase inhibition activity by the ligands. Two of the ligands showed IC_{50} values in the sub-micromolar range in the TRAP-LIG assay, which are the best among the benzimidazole derivatives reported so far. The ligands also exhibited cancer cell selective nuclear internalization, nuclear condensation, fragmentation, and eventually antiproliferative activity in long-term cell viability assays. Annexin V-FITC/PI staining assays confirm that the cell death induced by the ligands follows an apoptotic pathway. An insight into the mode of ligand binding was obtained from the molecular dynamics simulations.

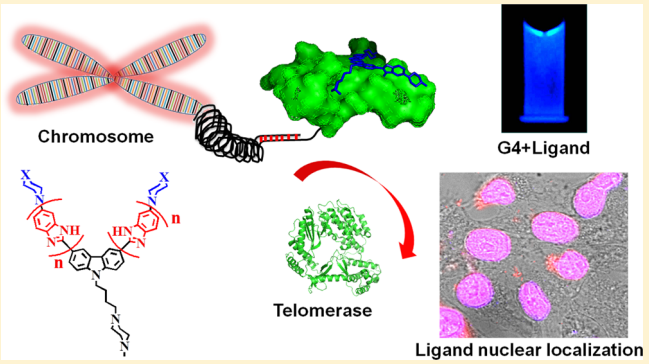

INTRODUCTION

Throughout the eukaryotic kingdom, the ends of linear chromosomes are capped by telomeres. The telomere in mammalian cells consists of a tandem repeat of guanine rich hexameric (5′-TTAGGG-3′) arrays of up to 5−15 kb from the extreme 3′-end.[1] In somatic cells, telomeres shorten due to the "end-replication problem" and consequently lead to various abnormalities of which the most important one involves an "end-to-end fusion".[2] A ribonucleoprotein complex called telomerase is responsible for telomeric length maintenance through the addition of TTAGGG repeats.[3] Initially identified in ciliates, human telomerase consists of three subunits: telomerase reverse transcriptase (hTERT), telomerase RNA (hTR), and Dyskerin. Certain types of cancer cells contain considerably high levels of telomerase activity, whereas it has not been detected in most of the normal somatic cells.[4] The terminal 3′-telomeric DNA sequence, being both single-stranded and G-rich in nature, has a high propensity to fold into the G4 structures by Hoogsteen H-bonding between the guanine bases under physiological ionic conditions.[5] The telomeric DNA folded into the G4 DNA is unable to serve as a substrate for telomerase. Therefore, stabilization of the G4 DNA is considered as a potential target in cancer chemotherapy.[6]

In recent years, a number of G4 DNA stabilizing small molecules has been synthesized and tested for telomerase inhibition. Among these, the natural product telomestatin[7] and the synthetic molecules, e.g., BRACO-19[8] and BMSG-SH-3,[9] are among the most promising candidates. Benzimidazole derivatives belong to another class of molecules which possess sequence-selective DNA binding ability.[10] These include Hoechst 33258 which is known for its specific affinity toward AT-rich minor grooves in double-stranded DNA. Neidle and co-workers demonstrated for the first time the symmetric bis-benzimidazoles for their potent sequence-specific duplex-DNA binding activity.[11] Li et al. were able to utilize a bis-(benzimidazole)pyridine derivative for selective G4 stabilization.[12]

We have previously reported 1,3-phenylene-bis-benzimidazole derivatives for their higher G4 DNA selectivity and stabilizing ability (Figure 1A).[13a−d] On the other hand, cationic carbazole derivatives are known for their ability to inhibit topoisomerase activity, and they also function as antimicrobial agents.[14] Recently, carbazole conjugates with a vinylic-pyridinium moiety were shown to bind and stabilize telomeric

Received: March 18, 2014

dx.doi.org/10.1021/jm500427n | J. Med. Chem. XXXX, XXX, XXX−XXX

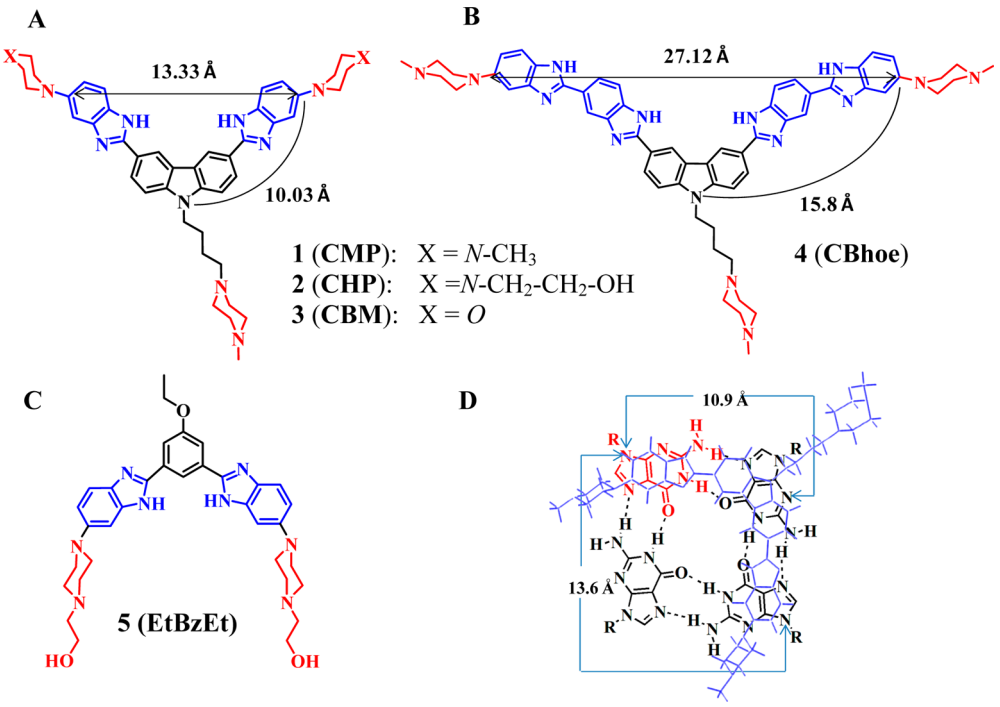

Figure 1. (A–C) The molecular structures of the ligands used in the study. (D) A superimposed structure of the G-tetrad[18] and the ligand (**1**) in real scale showing efficient overlapping. The ligand is shown in blue color. The *mono*-(bis-benzimidazole) derivatives (**1**–**3**) possess more similarity with the G-tetrad dimension than the corresponding *di*-(bis-benzimidazole) derivative (**4**).

DNA G-quadruplexes and inhibit telomerase activity.[15] A few carbazole–benzimidazole conjugates are known for the sequence-specific double-stranded DNA binding.[16] However, there is hardly any example of the G4 DNA selective ligands that inhibit telomerase activity in this family.[17] It occurred to us that it would be logical to modify carbazole–benzimidazole conjugates so that they are transformed into the G4 DNA binders and do not prefer the duplex DNA. Finally, they should also be capable of targeting the cancer cells selectively. Herein, we report the syntheses of four new benzimidazole derivatives with a carbazole core—**CMP** (**1**), **CHP** (**2**), **CBM** (**3**), and **CBhoe** (**4**)—and show that they possess a high potential for the G4 DNA stabilization. The structure–activity relationship has been investigated with functional variation from *mono*-(bis-benimidazole) to *di*-(bis-benzimidazole) along with different substitutions at the termini ranging from piperazine to morpholine (Figure 1). The variation in the number of benzimidazoles which leads to an alteration in the molecular dimension, the extent of crescent shape in the molecular structure, along with the modification in the end-functionality enabled us to investigate their influence on the G4 DNA binding and telomerase inhibition efficiency. Finally, the experimental results were rationalized with appropriate computational studies.

RESULTS AND DISCUSSION

Synthesis. Herein we have designed and synthesized benzimidazole derivatives based on carbazole as the central pharmacophore. We have considered a few aspects in the ligand design like the dimension, shape, extended planarity, and nature of protonatable sites to investigate their role in the structure–activity relationship. The molecular dimension and the crescent character of the ligands have been tuned by varying the number of benzimidazole units attached to the central carbazole core. To optimize their interaction with DNA, we have incorporated a piperazine/morpholine moiety in the three termini which should induce hydrogen bonding interactions and get protonated at pH 7.4 to facilitate the ligand's interaction with the phosphate groups of DNA.[19]

The synthesis started with the N-alkylation of carbazole upon reaction with 1,4-dibromobutane by the PTC method to furnish the *N*-4-bromobutyl-carbazole (**9**) in ∼72% yield. The bromo derivative (**9**) was then reacted with *N*-methylpiperizine followed by formylation of the carbazole nucleus to obtain the dialdehyde (**11**) in 75% yield. Oxidative coupling of **11** with each of the individual diamines **6**, **7**, and **8** in the presence of $Na_2S_2O_5$ afforded the final compounds **1**, **2**, and **3**, respectively, in 60–80% isolated yield (Scheme 1).

In a separate flask, 4-aminobenzonitrile was N-acetylated in 98% yield. This was followed by its nitration (85%) and the resulting product was then deacetylated to furnish 4-amino-3-nitrobenzonitrile (**14**) in 95% yield. The compound **14** was then reacted with dry HCl in the presence of freshly dried ethanol to afford the corresponding imino-ether hydrochloride (**15**) in 85% yield. The resulting compound **15** was reacted with freshly prepared diamine **6** to obtain the nitro amino benzimidazole derivative (**16**) in 78% yield. Subsequent reduction of compound **16** afforded the corresponding diamine (**17**) which was used for the next reaction without isolation. The coupling of freshly prepared diamine **17** with the dialdehyde (**11**) afforded the desired *di*-(bis-bezimidazole) derivative (**4**) in 50% yield (Scheme 2). All the new compounds were adequately characterized by IR, NMR, mass, and elemental analysis as given in the Materials and Methods.

UV–vis Absorption Spectral Titrations. To confirm whether each ligand interacts with the G4 DNA, UV–vis titrations of each compound with preformed G4 DNA were individually performed in 10 mM Tris–HCl (pH 7.4)

dx.doi.org/10.1021/jm500427n | J. Med. Chem. XXXX, XXX, XXX–XXX

Scheme 1[a]

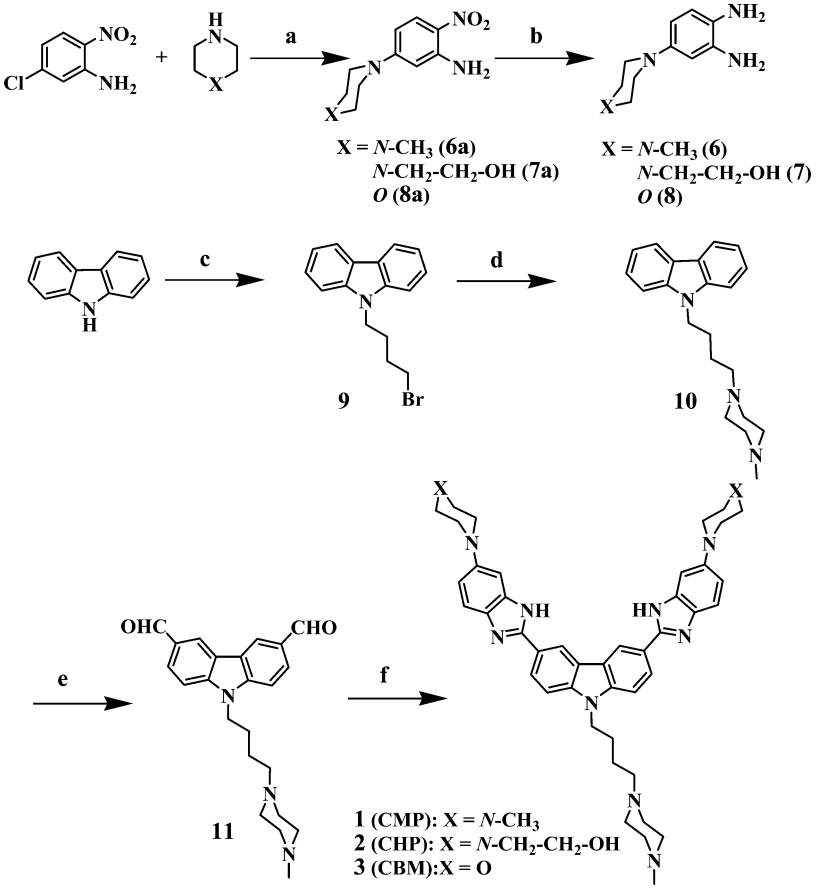

[a]Reagents, conditions, and yields: (a) K_2CO_3, dry DMF, 110 °C, 24 h, 89%; (b) Pd/C−H_2, EtOH, rt, 24 h; (c) 1,4-dibromobutane, TBAI, 50% NaOH, benzene, rt, 12 h, 72%; (d) *N*-methyl-piperazine, K_2CO_3, acetonitrile, rt, 6 h, 89%; (e) $ZnCl_2$, $POCl_3$/DMF, 0 °C → 100 °C, 24 h, 75%; (f) **6**, **7**, or **8**, $Na_2S_2O_5$, EtOH, 80 °C, 24 h, 60−80%.

containing 0.1 M NaCl or KCl and 0.1 mM EDTA. This was compared with their binding with a telomeric duplex DNA or calf-thymus (CT) DNA in 10 mM Tris−HCl (pH 7.4) containing 40 mM NaCl and 0.1 mM EDTA.

Ligand solutions of 5 μM were titrated by gradual addition of aliquots of preformed G4 DNA (50 μM). This resulted in a strong hypochromism, suggesting the involvement of π-stacking interactions between the ligands and the G4 DNA. The extent of hypochromicity observed with the duplex DNA (either telomeric duplex or CT DNA) during titration was insignificant, indicating considerably weaker interactions of the ligands with the duplex DNA (Supporting Information, Figures S1 and S2). The absorption spectral data (at 320 nm for each of **CMP**, **CHP**, and **CBM** and 340 nm for **CBhoe**) were analyzed using the linear Scatchard equation $r/C_f = K_a(n - r)$ and plotted to determine the binding constants (Table 1 and Supporting Information, Table S1) following a previously reported protocol (discussed in the Supporting Information).[13a−e]

Fluorescence Spectroscopy. Each ligand when solubilized in the experimental buffer of pH 7.4 displayed significant fluorescence emission following excitation at either 300 or 330 nm. Accordingly, we have used fluorescence spectroscopy to monitor the interaction of each ligand with the preformed G4 DNA in various buffer solutions in the presence of KCl or NaCl. All the ligands **CMP**, **CHP**, **CBM**, and **CBhoe** showed low fluorescence in Tris−HCl buffer possibly due to solvent induced collisional quenching in the aqueous medium (Figure 2A and B and Supporting Information, Figures S3 and S4). When an increasing amount of the preformed G4 DNA was added to the ligand solution in Tris−HCl buffer of pH 7.4, sharp increases in the fluorescence intensity were observed, which was followed by saturation for each ligand.

The increase in fluorescence intensity indicates that the ligands come to the proximity of the G4 DNA and achieve a hydrophobic environment to retain their intrinsic fluorescence emission manifesting their high affinity toward the G4 DNA. The extent of increments in the fluorescence emission was different for the ligands in buffer solutions according to their binding efficiency (Figure 2A and B and Supporting Information, Figures S3 and S4). Moreover, the ligands showed a higher enhancement in the fluorescence intensity in KCl buffer than the corresponding NaCl buffer possibly due to their higher affinity toward the K^+-ion-stabilized G4 DNA (Figure 2C and Supporting Information, Figures S5 and S6, Table S2). The fluorescence images showed selective light-up ability toward the G4 DNA upon ligand binding (Figure 2D and Supporting Information, Figure S7).

Each ligand solution was also titrated against CT DNA in 10 mM Tris−HCl (pH 7.4), 0.1 mM EDTA, and 40 mM NaCl. The titrations did not show any significant change in the fluorescence emission spectra (Figure 2C). This observation indicates the minimal affinity of the ligands toward the double-stranded CT DNA.

dx.doi.org/10.1021/jm500427n | J. Med. Chem. XXXX, XXX, XXX−XXX

Scheme 2[a]

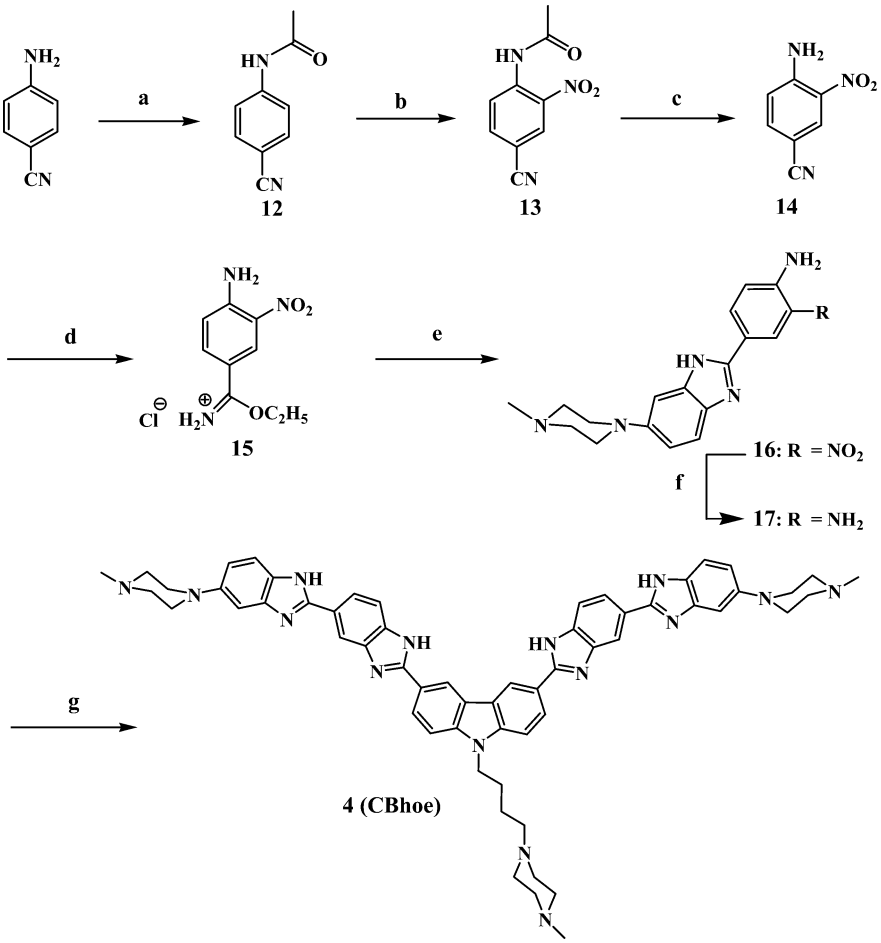

[a]Reagents, conditions, and yields: (a) Ac_2O (4 equiv), NaOAc, rt, 20 min, 98%; (b) KNO_3 (2.1 equiv), c. H_2SO_4, <0 °C, 1 h, 85%; (c) 10% H_2SO_4, heat, 30 min, 95%; (d) anhyd. HCl(g), dry EtOH, 7 days of stirring, rt, 85%; (e) 4-(4-methylpiperazin-1-yl)benzene-1,2-diamine (Scheme 1; compound **6**) EtOH:AcOH (2:1), reflux, 24 h, 78%; (f) Pd/C−H_2, EtOH, rt, 12 h, 100%; (g) 9-(4-(4-methylpiperazin-1-yl)butyl)-9*H*-carbazole-3,6-dicarbaldehyde (Scheme 1; compound **11**), $Na_2S_2O_5$, EtOH, 80 °C, 12 h, 50%.

Table 1. Dissociation Constants (K_d) of the Ligands with the Preformed Hum_{21} G4 DNA and CT DNA

	Hum_{21} (NaCl)[a]		Hum_{21} (KCl)[a]		CT DNA[b]	
ligand	K_d (μM)	*n*	K_d (μM)	*n*	K_d (μM)	selectivity toward the G4 DNA over the duplex DNA
CMP	0.34 ± 0.01	2.5	0.13 ± 0.01	2.7	196 ± 12	576
CHP	0.05 ± 0.002	2.3	0.03 ± 0.002	3.2	25 ± 2	500
CBM	0.48 ± 0.02	2.9	0.33 ± 0.04	2.6	312 ± 14	650
CBhoe	0.38 ± 0.03	3.2	0.23 ± 0.02	3.4	89 ± 4	234

[a]Dissociation constants (K_d) were calculated from the binding assays performed with the preformed Hum_{21} G4 DNA in 10 mM Tris−HCl (pH 7.4) having 0.1 M NaCl/KCl and 0.1 mM EDTA. The notation "*n*" represents the binding stoichiometry of the ligands with the G4 DNA. [b]Binding assays were performed with CT DNA in 10 mM Tris−HCl (pH 7.4) having 40 mM NaCl and 0.1 mM EDTA.

G4-FID Assays. Fluorescent intercalator displacement assays have been performed to examine each ligand's relative affinity toward the G4 DNA and selectivity over the double-stranded CT DNA or telomeric duplex DNA. For this purpose, the standard G4 DNA intercalator thiazole orange (TO) has been used.[20] All the ligands showed efficient TO displacement ability from the G4 DNA−TO complex. The *mono*-(bis-benzimidazole) ligands (**CMP**, **CHP**, and **CBM**) showed a higher efficiency than the *di*-(bis-benzimidazole) ligand (**CBhoe**), suggesting a higher G-tetrad affinity of the former ligand (Figure 3). In contrast, all the ligands showed a considerably lower TO displacement efficiency (Table 2) while interacting with the duplex DNA (CT DNA and Telo ds DNA).

Circular Dichroism Spectroscopy. The preformed Hum_{21} G4 DNA structures were established by recording their CD spectra both in 0.1 M NaCl and 0.1 M KCl buffer. These spectral profiles were consistent with those reported earlier.[21,22] The G4 DNA in the KCl buffer showed a negative peak at 240 nm and a positive peak at 292 nm along with two shoulders at 250 and 270 nm which matched with the reported intramolecular hybrid DNA structure as described earlier.[19] The G4 DNA in NaCl buffer showed two positive peaks at 295 and 246 nm along with a negative peak at 266 nm which is similar to

dx.doi.org/10.1021/jm500427n | J. Med. Chem. XXXX, XXX, XXX−XXX

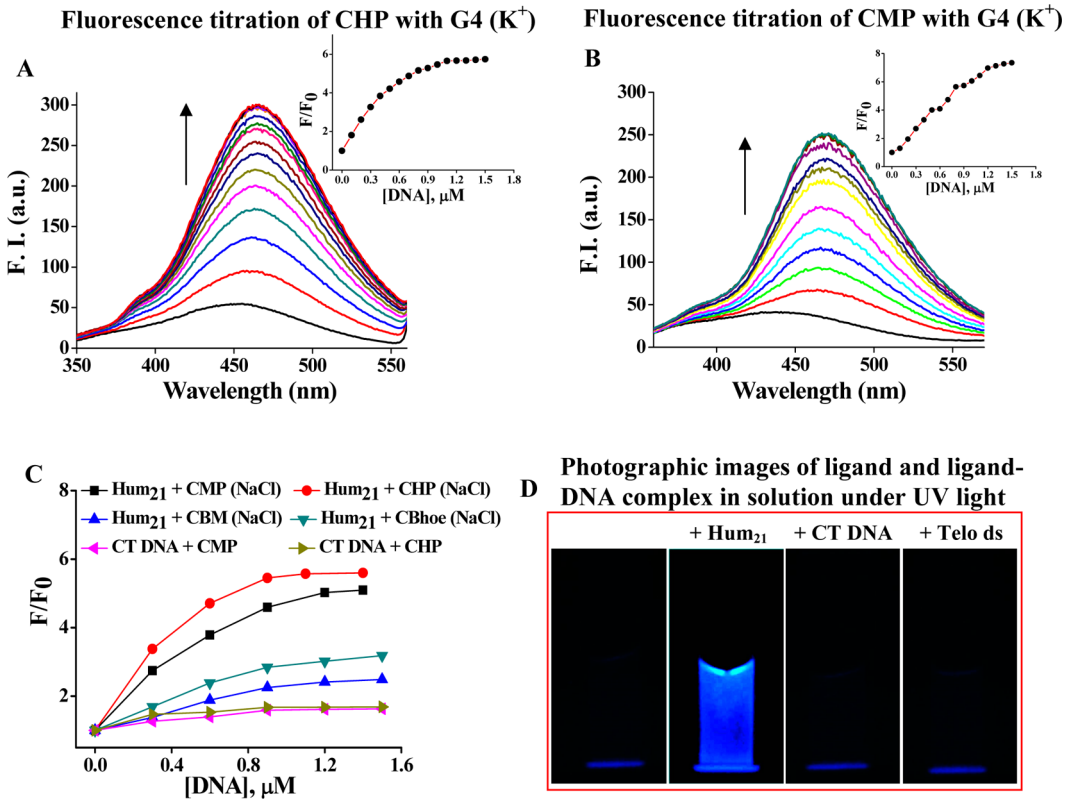

Figure 2. Fluorescence titration spectra of 0.4 μM ligand (A) **CHP** and (B) **CMP** in 10 mM Tris–HCl (pH 7.4), 0.1 mM EDTA, and 0.1 M KCl with 10 μM preformed Hum_{21} G4 DNA. (C) Relative enhancement in the fluorescence intensities of the ligands (**CMP**, **CHP**, **CBM**, and **CBhoe**) in 10 mM Tris–HCl (pH 7.4), 0.1 mM EDTA, and 0.1 M NaCl upon interaction with the Hum_{21} G4 DNA/CT DNA. (D) Fluorescence images of 20 μM ligand **CHP** and ligand–DNA complexes (with 40 μM Hum_{21}, CT DNA, and Telo ds DNA) under UV light (λ_{ex} = 365 nm) in 10 mM Tris–HCl (pH 7.4) and 0.1 mM EDTA having either 0.1 M KCl (for G4 DNA) or 0.04 M NaCl (for CT DNA and Telo ds DNA).

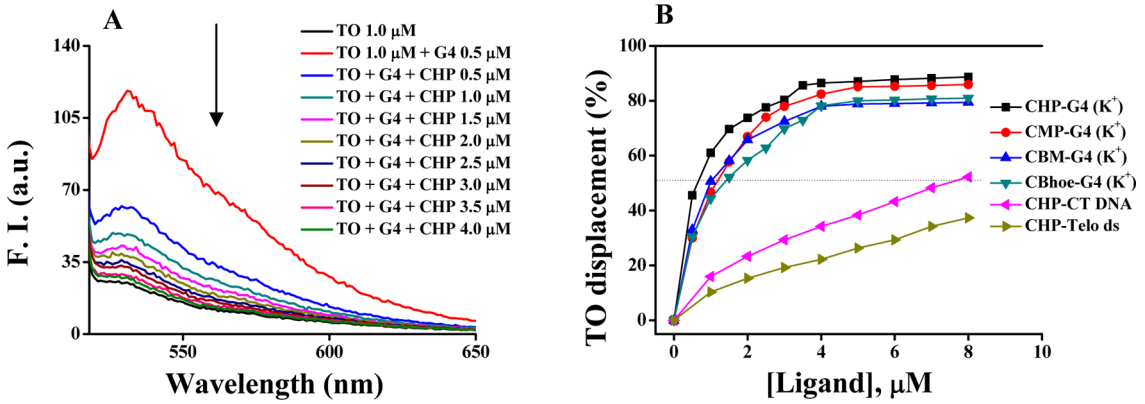

Figure 3. (A) TO displacement assay by the ligand **CHP** from Hum_{21} G4 DNA–TO complex. (B) Relative TO displacement plots for the ligands **CMP**, **CHP**, **CBM**, and **CBhoe**.

Table 2. DC_{50} Values (Ligand Concentrations for the Displacement of 50% of the Bound TO from DNA) of the Ligands as Determined from Fluorescent Intercalator Displacement Assays[a]

ligand	DC_{50} (μM)	ligand	DC_{50} (μM)
CMP (G4-K+)	0.61 ± 0.04	**CBM (G4-K+)**	1.01 ± 0.03
CHP (G4-K+)	1.12 ± 0.03	**CBhoe (G4-K+)**	1.36 ± 0.05
CHP (CT DNA)	7.71 ± 0.08	**CHP (Telo ds)**	>8

[a]The results are the average of two independent experiments.

that reported for an intramolecular antiparallel G4 DNA structure in solution.[22]

The titration of the G4 DNA with both **CMP** and **CHP** led to an increase in the positive peak at 295 nm followed by the appearance of a new peak in the range of the ligand's absorption maxima (300–350 nm) at higher ligand concentrations (Figure 4 and Supporting Information, Figures S8 and S9). **CBM** and **CBhoe** also showed sharp enhancements in the CD intensity, emphasizing their strong association with the G4 DNA structure (Supporting Information, Figure S9C and D). Though the spectra maintained an iso-dichroic point in the initial stage of titration, they started to deviate at higher ligand

dx.doi.org/10.1021/jm500427n | J. Med. Chem. XXXX, XXX, XXX–XXX

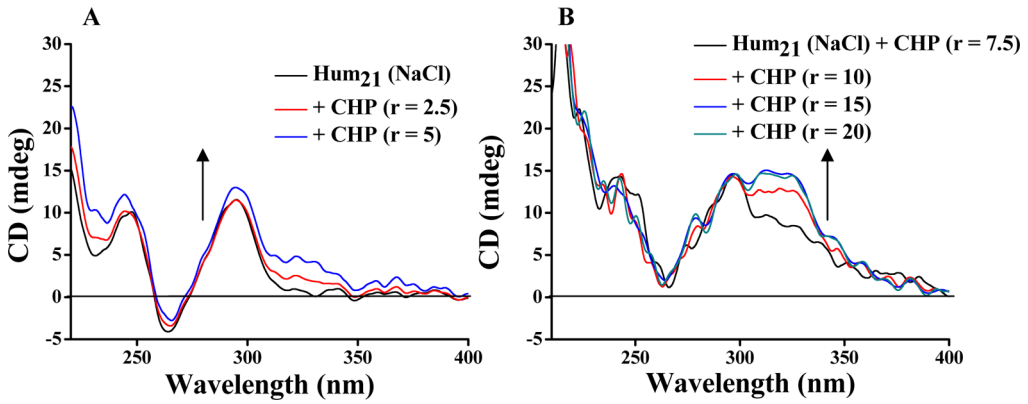

Figure 4. (A, B) CD spectral titrations of 4 μM Hum_{21} G4 DNA with increasing concentration of **CHP** in 10 mM Tris−HCl (pH 7.4) containing 0.1 mM EDTA and 0.1 M NaCl.

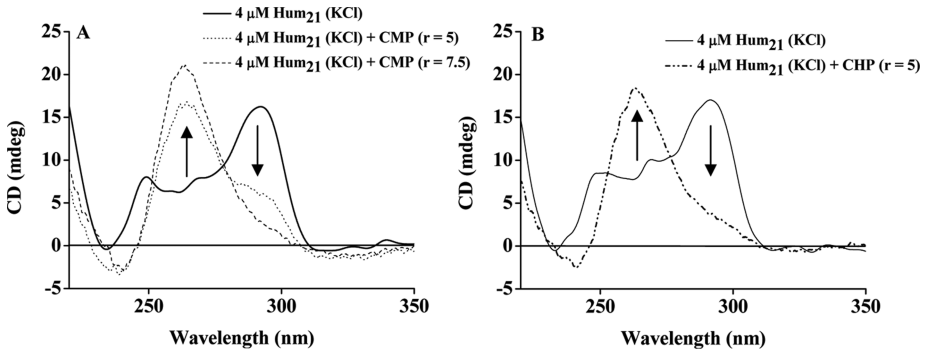

Figure 5. Formation of the G4 DNA in the presence of (A) **CMP** and (B) **CHP** in 10 mM Tris−HCl (pH 7.4), 0.1 M KCl, and 0.1 mM EDTA.

concentrations with simultaneous appearance of an induced circular dichroism (ICD) band (Figure 4). This suggests the generation of more than one form of DNA−ligand complexes possibly due to the groove binding at higher ligand concentrations. For all the ligands, the ICD started appearing from a [L]:[DNA] ratio of ∼5. Most probably at lower concentration, the ligands prefer to interact with the G-tetrad of the G4 DNA structure, whereas, at a higher concentration of the ligands, these molecules begin to interact with the chiral groove and the chirality gets transferred to the DNA groove bound achiral ligands, giving ICD followed by saturation.[13a−e]

The CD titration of CT DNA with each of the ligands **CMP**, **CHP**, and **CBM** did not, however, show any significant change. This indicates their poor binding affinity toward the duplex DNA (Supporting Information, Figure S8C). In contrast, the ligand **CBhoe** showed appreciable enhancement in the ICD region upon binding with CT DNA (Supporting Information, Figure S8D). Thus, the CD spectral titration studies with both the G- quadruplex and the duplex DNA suggest that the ligands containing one (bis-benzimidazole) moiety have better selectivity toward the G4 DNA than the ligands consisting of two (bis-benzimidazole) units.

Formation of the G4 DNA in the Presence of the Ligand. When the G4 DNA was formed in the presence of ligand **CMP** or **CHP** (at the [L]:[DNA] ratio of 7.5) in NaCl buffer, the positive peak at 295 nm did not shift, except that there was a change in the peak intensity. However, the positive peak at 246 nm showed an ∼3 nm red-shift with intensity changes in both cases. Additionally, there was a chirality inversion in the region of the negative peak around 266 nm along with a large red-shift of about 13 nm. Probably the Na^+-stabilized antiparallel G4 DNA structure is maintained with some distortion in the parent G4 structure due to the strong association with the ligands (Supporting Information, Figure S10A and B).

Surprisingly, in KCl buffer, the phenomenon was totally different. Both of the ligands showed structural inversion from the K^+-stabilized mixed hybrid G4 DNA structure to a stable, biologically nonrelevant, telomeric parallel G4 DNA structure.[23] The positive peaks at 292, 271, and 251 nm merged together to give a positive peak at 263 nm and a negative peak at 241 nm, indicating the formation of the parallel G4 DNA (Figure 5 and Supporting Information, Figure S11). Though telomeric G4 DNA is known to form a hybrid structure under physiological conditions, it has been shown to adopt a parallel conformation in a molecularly overcrowded environment.[23,24] Interestingly, for **CMP** at [L]:[DNA] = 5, the presence of the 292 nm peak provides evidence of incomplete structural inversion, whereas, at [L]:[DNA] = 7.5, the inversion was complete. We note that **CHP** showed a lower ligand concentration ([L]:[DNA] = 5) for the complete structural inversion. The ligand **CBhoe** also showed a similar phenomenon, but the topological transformation was incomplete even at [L]:[DNA] = 7.5 (Supporting Information, Figure S10D). Interestingly, the ligand **CBM** did not show any kind of structural inversion (Supporting Information, Figure S10C). Thus, the studies suggest that the two terminal piperazines attached next to the benzimidazole moiety (**CMP**, **CHP**, and **CBhoe**) are essential for the topological transformation.

DNA Melting Studies. We incubated the preformed G4 DNA with each of **CMP**, **CHP**, **CBM**, and **CBhoe** separately either in NaCl or KCl buffer for 12 h and determined their

dx.doi.org/10.1021/jm500427n | J. Med. Chem. XXXX, XXX, XXX−XXX

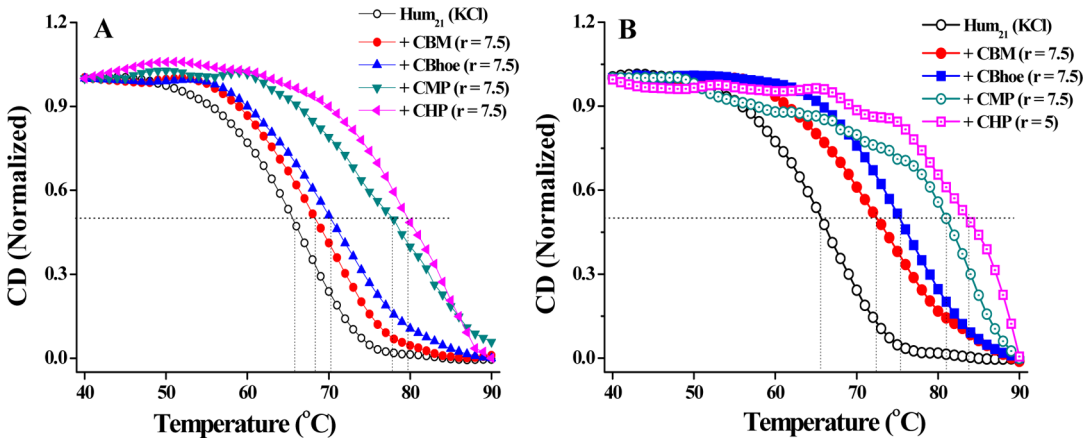

Figure 6. (A) Melting profiles of the preformed G4 DNA alone and the G4 DNA incubated with ligands for 12 h in specified concentrations in KCl buffer, monitored at a wavelength of 295 nm. (B) Melting profiles of the preformed G4 and the G4 DNA formed in the presence of specified ligand with indicated concentrations in KCl buffer, monitored at a wavelength of either 295 nm (for **CBM**) or 263 nm (for **CMP**, **CHP**, and **CBhoe**).

Table 3. Summary of the DNA Melting Studies[a]

ligand	NaCl (preformed), ΔT_m (°C)	NaCl (with ligand), ΔT_m (°C)	KCl (preformed), ΔT_m (°C)	KCl (with ligand), ΔT_m (°C)
CMP	7	12	13	16
CHP	10	15	15	19
CBM	4	8	4	7
CBhoe	7	10	7	10

[a] ΔT_m values were obtained from the differences in the melting temperatures of the ligand bound and uncomplexed G4 DNA in 10 mM Tris−HCl (pH 7.4) containing 0.1 M KCl/NaCl and 0.1 mM EDTA. The results are the average of two independent experiments and are within ±0.5 °C of each other.

thermal denaturation profile by following the changes in CD spectral profiles as a function of temperature. Also, we checked the melting data of the G4 DNA formed in the presence of ligand in both NaCl and KCl buffers. The melting experiments for the mixed-hybrid G4 DNA in KCl buffer and antiparallel basket type G4 DNA in NaCl buffer incubated with each of the ligands separately afforded sigmoidal melting curves at 295 nm, indicating significant enhancement in the melting temperature compared with that of the G4 DNA alone (Figure 6 and Supporting Information, Figure S12A and B). Similarly, the melting experiments for the G4 DNA formed in the presence of each ligand in NaCl buffer were performed at 295 nm.

On the other hand, the melting studies in KCl buffer were followed at 263 nm because of the peak shift due to a structural alteration in the presence of **CMP**, **CHP**, and **CBhoe** (Figure 5). A [L]:[DNA] ratio of ∼7.5 was used for **CMP** and **CBhoe**, which showed a total structural inversion in KCl buffer, whereas for **CHP** the corresponding ratio is ∼5 in KCl buffer and ∼7.5 in NaCl buffer (Figure 5 and Supporting Information, Figure S11D).

All the CD melting experiments showed significant thermal stabilization of the G4 DNA formed in the presence of each ligand, compared to the G4 DNA alone (Table 3). Upon increasing the ligand concentrations from r = 5 to r = 7.5, the denaturation temperatures of the G4 DNA also increased (Supporting Information, Figure S13). The elevated thermal stabilization may have originated from the additional groove binding at higher ligand concentrations which is also evident from the concomitant appearance of the ICD band.[25] The melting curves of the preformed G4 DNA incubated with each of the individual ligands showed hysteresis in the reverse scan (Supporting Information, Figure S12C). This was possibly due to the formation of the G4 structure in a kinetically slower process. Interestingly, the G4 DNA formed in the presence of **CMP**, **CHP**, and **CBhoe** did not show any hysteresis in the reverse melting scan. This phenomenon may be explained considering the formation of thermodynamically and kinetically more stable parallel G4 DNA structures (Supporting Information, Figure S12D).

S1 Nuclease Assay. A single-stranded DNA can adopt various secondary structures like A-motif, i-motif, G-quadruplex, etc., depending upon its sequence and experimental conditions.[26] Topology specific interaction is a useful technique in the identification of DNA secondary structures. S1 is an endonuclease which cleaves preferentially the single-stranded DNA over the duplex DNA, G4 DNA, and i-motif DNA in the presence of Zn^{2+} ion.[27]

We observed that the Hum_{21} ODN even in the presence of 50 mM KCl (Figure 7, lane 1) was sufficiently cleaved, suggesting that the G4 DNA was not stable and remained in equilibrium with its random single-stranded form. The two lower major bands represent the extent of highly cleaved ODN products. However, as we incubated the ODN in 50 mM KCl along with increasing concentration of each ligand (lanes 2−6), the lower bands corresponding to highly digested products were reduced significantly, indicating protection from the S1 nuclease cleavage. The ss-DNA (Figure 7, lane 7) was unable to resist the S1 nuclease induced cleavage, giving two intensely populated bands of higher mobility. Thus, this study provides additional evidence in support of the G4 DNA stabilizing capability of the ligands.

TRAP-LIG Assay. A modified TRAP assay was performed using a three-step Telomeric Repeat Amplification Protocol (TRAP-LIG) procedure.[28] This involved (1) primer elongation by telomerase in the presence and absence of ligand, (2) removal of the bound and unbound ligand from the elongated

dx.doi.org/10.1021/jm500427n | J. Med. Chem. XXXX, XXX, XXX−XXX

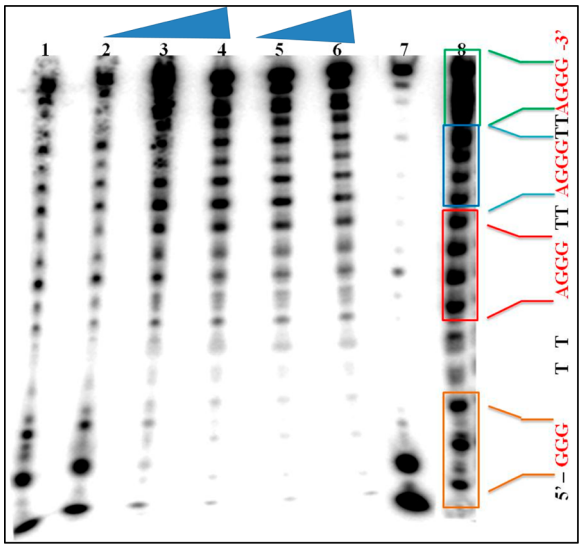

Figure 7. S1 nuclease cleavage of the human telomeric G4 DNA in the presence and absence of **CMP** and **CHP**. Lane 1: Hum_{21} in 50 mM KCl. Lanes 2, 3, and 4: Hum_{21} + **CMP** (2.5, 5, and 7.5 μM) in 50 mM KCl. Lanes 5 and 6: Hum_{21} + **CHP** (2.5 and 5 μM) in 50 mM KCl. Lane 7: Hum_{21} in the absence of KCl (single strand). Lane 8: A+G ladders corresponding to the Hum_{21} DNA.

primer, and (3) PCR amplification of the telomerase elongated product, as given below.

Since telomerase is a potential drug target toward the anticancer therapy, we examined the efficiency of the synthesized ligands **CMP**, **CHP**, **CBM**, and **CBhoe** toward telomerase inhibition by modified three-step TRAP-LIG assay.[28] Ligands were tested at concentrations ranging from 0.01 to 5 μM for their ability to inhibit the telomerase activity against the telomerase enzyme extracted from the human lung carcinoma A549 cell lines in vitro. Both the ligands **CMP** and **CHP** showed total inhibition at ~1 μM ligand concentration (Figure 8), whereas **CBhoe** and **CBM** showed a total inhibition

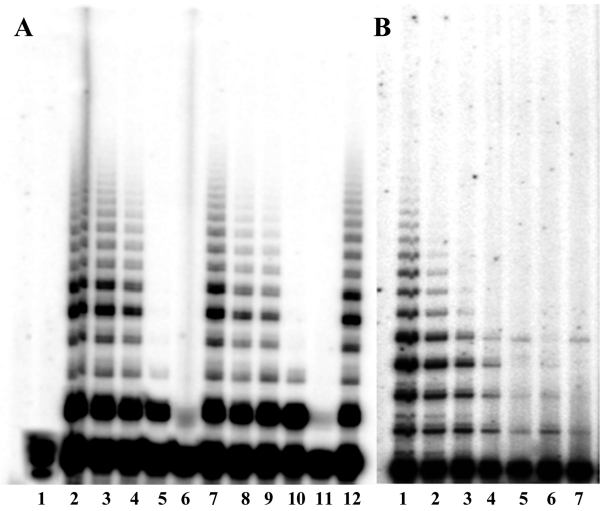

Figure 8. (A) Lane 1: Negative control (absence of enzyme and ligand). Lane 12: positive control. Lanes 2, 3, 4, 5, and 6: with increasing concentrations of **CMP** (0.01, 0.1, 0.2, 1, and 3 μM). Lanes 7, 8, 9, 10, and 11: with increasing concentrations of **CHP** (0.01, 0.1, 0.2, 1, and 3 μM). (B) Lane 1: positive control. Lanes 2, 3, 4, 5, 6, and 7: with increasing concentrations of **CBM** (0.5, 1, 2, 3, 4, and 5 μM).

at ~3 μM (Supporting Information, Figure S14A). To the best of our knowledge, the present set of compounds **CMP** and **CHP** are the most potent telomerase inhibitors in the bis-benzimidazole category. The quantification in UVI-Tech gel documentation station using UVI-Band Map software (version 97.04) enabled determination of the IC_{50} values for **CMP**, **CHP**, **CBM**, and **CBhoe** which were 0.9, 0.6, 1.6, and 1.8 μM, respectively (Table 4 and Supporting Information, Figure S14B).

Table 4. IC_{50} Values Calculated from the TRAP-LIG Assay[a]

ligand	IC_{50} (μM)	ligand	IC_{50} (μM)
CMP	0.9 ± 0.02	**CBM**	1.6 ± 0.02
CHP	0.6 ± 0.01	**CBhoe**	1.8 ± 0.03

[a]The results are the average of two independent experiments.

Cancer-Cell-Specific Toxicity. The cytotoxicity studies of the ligands (**CMP**, **CHP**, **CBM**, and **CBhoe**) were performed in telomerase negative human foreskin fibroblast normal cells (HFF),[29] representative cancer cells (adenocarcinomic human alveolar basal epithelial cells—A549, human cervical cancer cells—HeLa, and human embryonic kidney transformed cells—HEK 293T, to demonstrate their cancer cell specificity in a short-term (72 h) cell viability assay.

At first, the cell viability experiments were performed in mortal HFF cells where no noticeable reduction in cell viabilities was observed in the presence of ligands (Figure 9 and Supporting Information, Figures S15 and S16). On the other hand, we noticed a significant decrease in cell viability in cancer cells at the same concentrations under identical conditions (Figure 9 and Supporting Information, Figures S15 and S16).

Long-Term Cell Viability Assay. It must be noted that the ligand's moderate toxicity to the cancer cells (IC_{50} ~8 μM) in a short-term (72 h) viability assay cannot be correlated with their activity through a telomerase inhibition pathway.[30] Therefore, long-term cell viability assays (15 days), which allow for a sufficient time tag for telomere shortening to take place, were performed using a sub-cytotoxic ligand concentration of 2 and 5 μM. Long-term cell proliferation experiments were carried out using human cervical cancer cells (HeLa) and human embryonic kidney transformed cells (HEK 293T).

All the ligands showed effective antiproliferative activity in accordance with their activity observed in a short-term cell viability assay. The ligands **CMP** and **CHP** were found to be more efficient than **CBM** and **CBhoe** toward this end (Figure 10 and Supporting Information, Figure S15C and D). Thus, such ligand's acute activity in a long-term (15 days) cell viability assay further confirms the possibility of a telomerase inhibition pathway. This observation suggests that the telomerase activity, which is more pronounced in cancer cells, may be targeted efficiently with these G-quadruplex DNA binding ligands.[31]

Annexin V-FITC and PI Staining Assay. To further ascertain whether the nature of ligand induced cell death was caused due to an apoptotic pathway, an Annexin-V and PI dual staining assay was performed to detect the presence of apoptotic cells after the treatment with ligands. Interestingly, for HeLa cells treated with ligands (10 μM **CHP** and **CMP**) for a period of 12 h, significant evidence of apoptosis was obtained. Ligand **CHP** and **CMP** showed ~55 and ~25% apoptotic cell populations, respectively. In contrast, HeLa cells not treated with any of the ligands (control) did not show any evidence of

dx.doi.org/10.1021/jm500427n | J. Med. Chem. XXXX, XXX, XXX–XXX

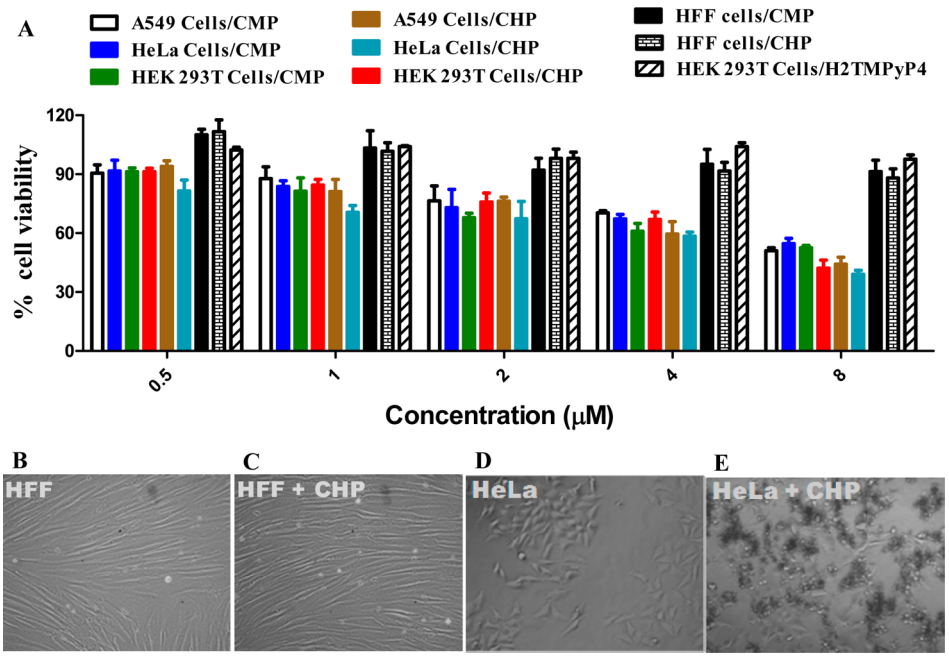

Figure 9. Effect of **CMP** and **CHP** on the cell viability after a short-term exposure (72 h) to different (A) cancer (A549, HeLa, and HEK 293T) cells and human foreskin fibroblast (HFF) normal cells as measured using the MTT assay. Cells were treated with each concentration in triplicates in individual experiments, and the results shown are based on at least three independent experiments. Representative bright field images of the cell morphology of human foreskin fibroblast (HFF) normal cells (B) before and (C) after the treatment with 4 μM **CHP** and HeLa cells (D) before and (E) after the treatment with 4 μM **CHP**.

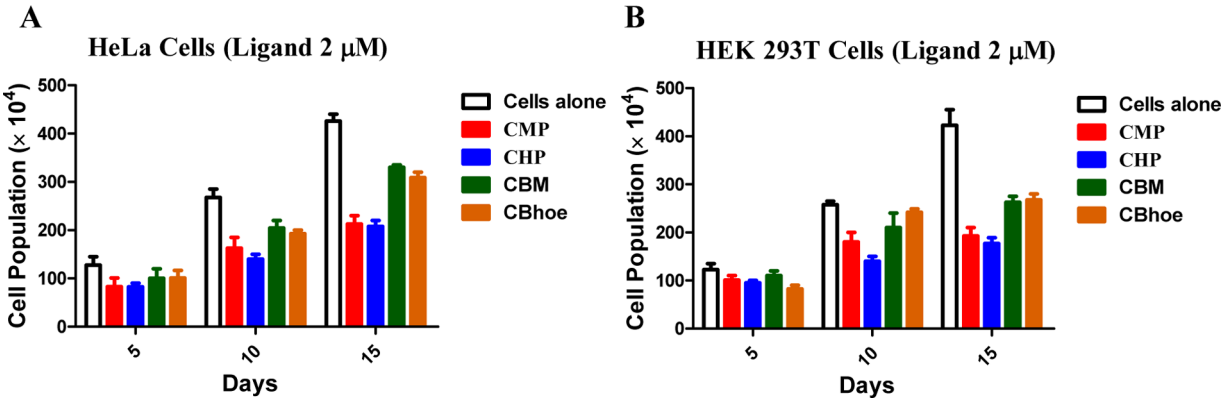

Figure 10. Effect of ligands on the cell viability upon long-term exposure (15 days) to (A) human cervical cancer cells (HeLa) and (B) human embryonic kidney transformed cells (HEK 293T) as measured using the MTT assay.

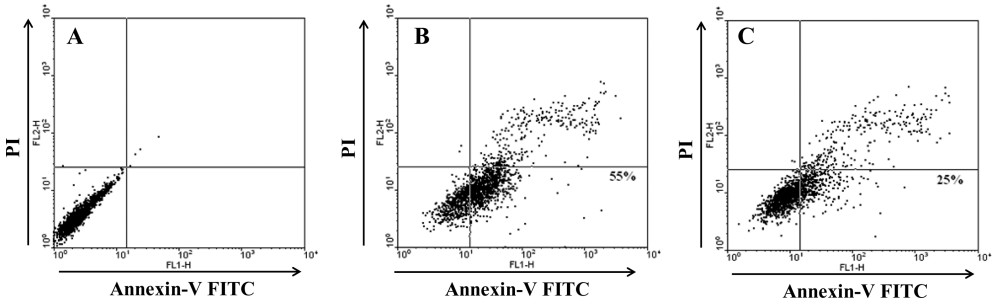

Figure 11. Representative dot plots for Annexin-V and PI staining of (A) untreated cells (HeLa) as control and after incubation with ligands (B) **CHP** and (C) **CMP**. The different stages of cells were assigned as alive (LL), early apoptotic (LR), late apoptotic (UR), and necrotic cells (UL). The depiction of apoptotic cell population is made in the lower right quadrant which originated due to the Annexin V-FITC staining only.

apoptotic cell populations (Figure 11). These observations suggest that the ligand induced cell death was primarily due to apoptosis consistent with an earlier report.[32]

Confocal Microscopy. To provide visual evidence, confocal microscopy experiments were performed to follow the cellular internalization of ligands. This also afforded critical

dx.doi.org/10.1021/jm500427n | J. Med. Chem. XXXX, XXX, XXX−XXX

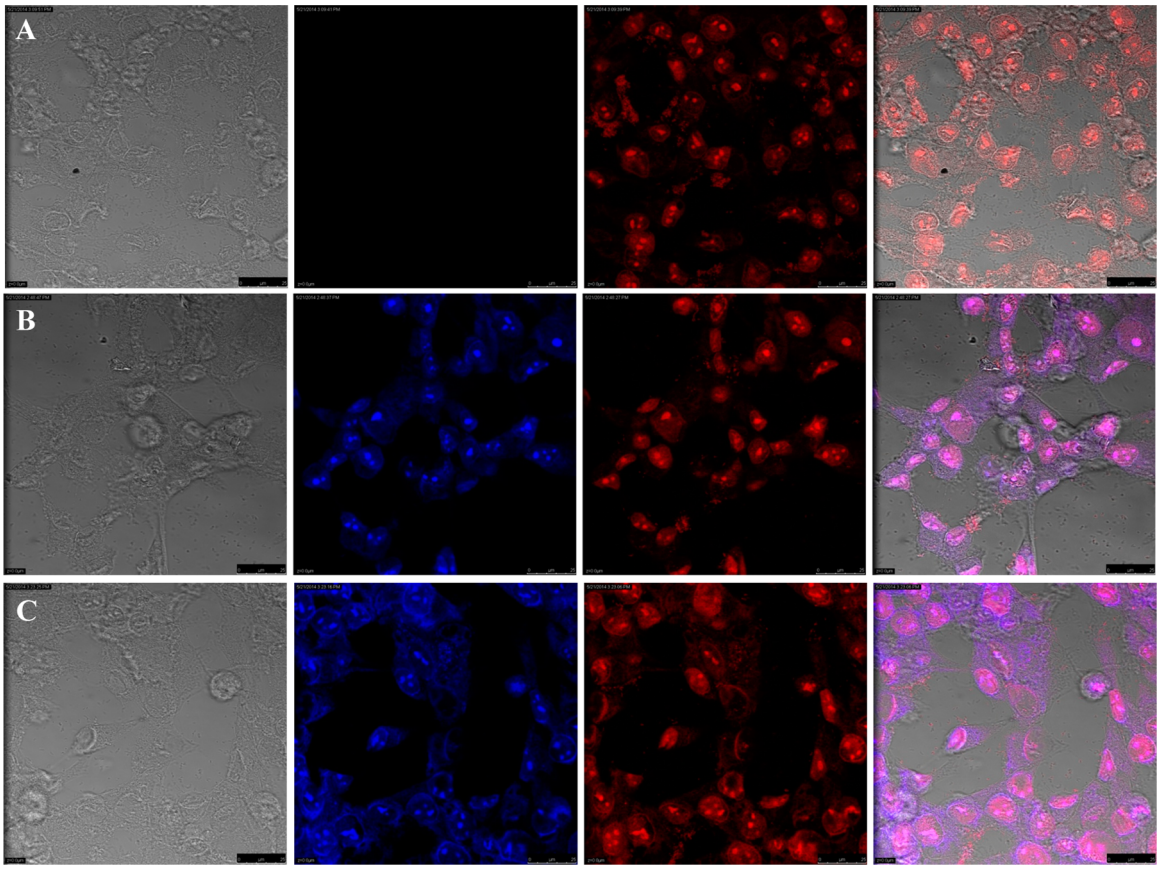

Figure 12. Representative confocal microscopic images depicting untreated cells (A) and cellular internalization of ligands at a concentration of 10 μM **CHP** (B) and **CMP** (C) for 12 h in HeLa cells. PI was used as a nuclear counterstain. Panels A, B, and C represent (left to right) bright field, ligand fluorescence (blue), PI nuclear counterstain (red), and overlay of the previous three images.

evidence toward differences in cell death induced by apoptosis in various cells. The ligand treated HeLa cells showed a prominent nuclear localization after 12 h of incubation (Figure 12). Nuclear localization of ligands was confronted using PI (propidium iodide) as a nuclear counterstain. On the other hand, normal HFF cells treated with ligands showed only cytoplasmic distribution (Supporting Information, Figure S17).

To identify the apoptotic cells as a result of the ligand treatment, PI was used to counterstain the nuclei (Figure 13). Condensed and fragmented nuclei were observed in ligand treated HeLa cells, which is a characteristic appearance of the apoptotic cells (Figure 13B, C, E, and F). On the contrary, we did not notice any change in the nuclear morphology of normal HFF cells treated with ligands under the same conditions (Figure 13H, I, K, and L).

Computational Studies. Each ligand possesses a planar aromatic moiety connected via C−C single bonds, and this makes the molecule flexible. The three pendent flexible piperazine/morpholine residues also contribute to the molecular features being dynamic in shape. Initially, the molecular structures were energy optimized using the B3LYP level of theory with 6-31G* as the basis set in Gaussian 03.[33] The energy optimized structures show that the central pharmacophore which consists of three aromatic residues is quite planar in nature. The two piperazine/morpholine residues connected to the benzimidazole moiety remain in the molecular plane. The pendant butyl-piperazine spacer attached to the carbazole-*N* projects out of the central molecular plane.

The MD simulation was performed using the Amber 9[34] software package with a 6 ns production run (Figure 14 and Supporting Information, Figure S19). The molecule **CMP** was found to prefer stacking in the 3′-end. The central pharmacophore is stacked over the G-quartet DNA plane, whereas the three piperazine arms approach the grooves interacting with the anionic phosphodiester backbone (Figure 14). Though a 1:1 ligand−DNA interaction shows stacking as the preferable interaction over the groove binding, at higher ligand concentrations, the ligand may also interact with the grooves, which has been experimentally observed with the manifestation of the ICD bands (Figure 5).[15,25,35] Hence, the MD simulation studies demonstrate the various types of possible interaction in favor of the strong G4 DNA binding efficiency of each ligand.

CONCLUSIONS

In this work, we present the design and synthesis of four novel carbazole based benzimidazole derivatives. We have investigated their interaction with the Hum_{21} G4 DNA by various techniques under different experimental conditions including physical, biological, and theoretical approaches. We have unambiguously shown that all the compounds are highly effective in the stabilization of preformed Hum_{21} G4 DNA structure. The *mono*-(bis-benzimidazole) derivatives (**CMP**, **CHP**, and **CBM**) showed a higher preference (>500-fold) toward the G4 DNA over the duplex DNA than the corresponding *di*-(bis-benzimidazole) ligand, **CBhoe**. Similarity in the molecular dimension of *mono*-(bis-benzimidazole)

dx.doi.org/10.1021/jm500427n | J. Med. Chem. XXXX, XXX, XXX−XXX

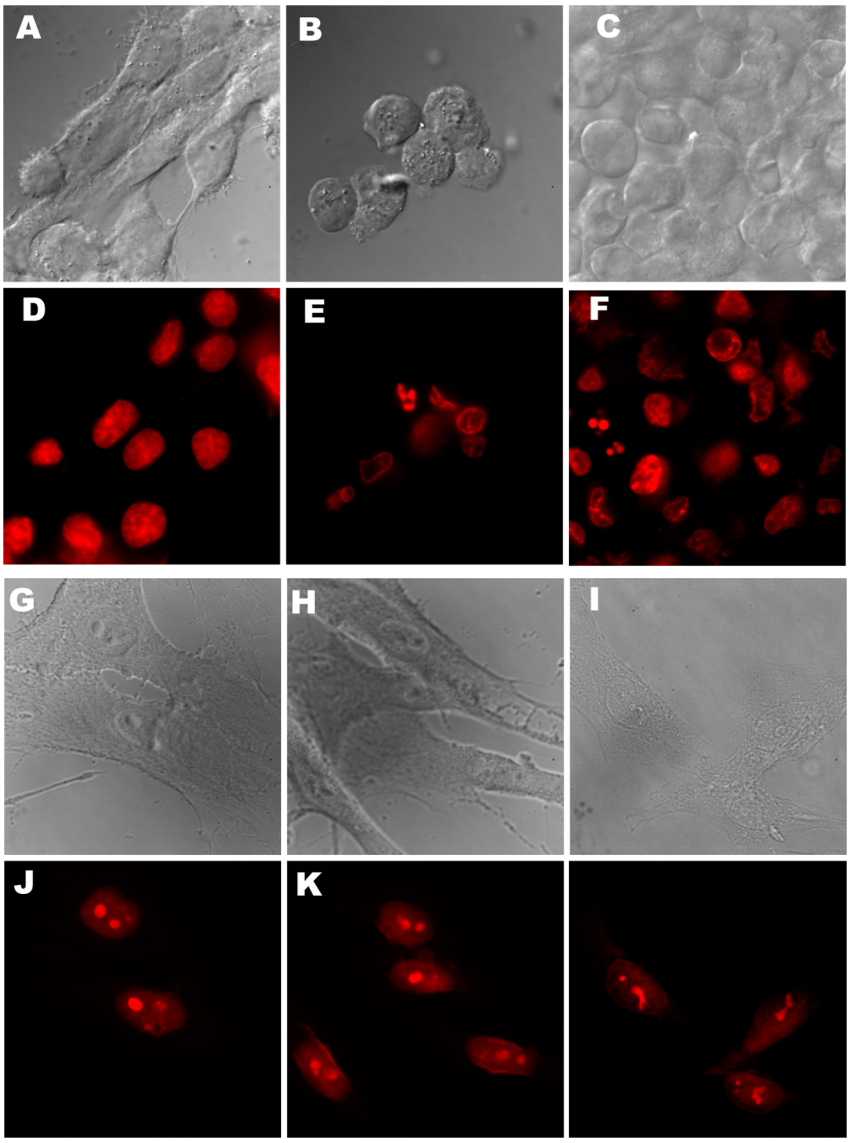

Figure 13. Representative bright field (A–C, HeLa cells; G–I, HFF cells) and fluorescence microscopic images (D–F, HeLa cells; J–L, HFF cells) of cells using PI as a nuclear counterstain. Parts A, D, G, and J show images of cells without ligand treatment, and parts B, E, H, and K and C, F, I, and L show images of cells treated with ligand **CHP** and **CMP** (10 μM), respectively, for 24 h.

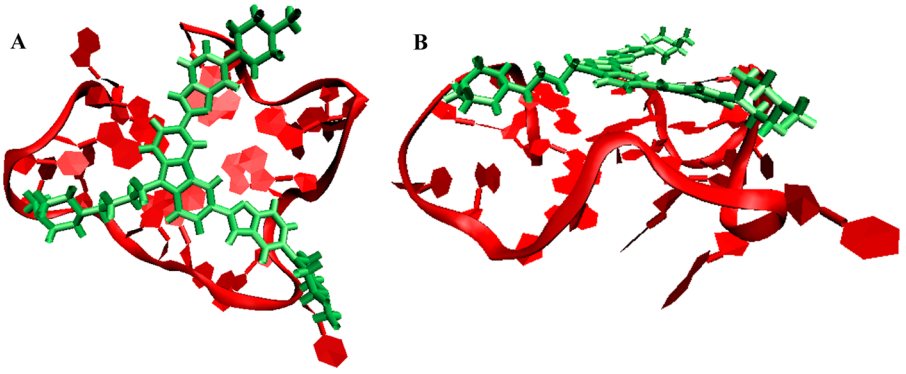

Figure 14. (A) Simulated structures of **CMP** and Hum_{21} G4 DNA (PDB 1KF1) DNA showing excellent stacking capability of the central pharmacophore while its side-arms interact with the grooves. The ligand is shown in stick model and is green in color, and the DNA is shown in red. (B) The side-view of the simulated complex shows that the ligand conserves its planarity while stacking upon the planar G-tetrad.

derivatives and G-tetrad may account for their higher selectivity toward the G4 DNA. On the other hand, the extended crescent shape in the molecular structure of the *di*-(bis-benzimidazole) ligand, **CBhoe**, could be responsible for its inferior structural

dx.doi.org/10.1021/jm500427n | *J. Med. Chem.* XXXX, XXX, XXX–XXX

discrimination ability between the G4 DNA and the duplex DNA. The observation of excellent fluorescence emission enhancement upon binding to the G4 DNA may be useful for the staining of DNA stretches that form G4 structures in vivo.[36] The ligands stabilize both the preformed hybrid and antiparallel G4 structures, rendering increases in their melting temperatures. The ligands containing three piperazine residues (**CMP**, **CHP**, and **CBhoe**) induced a structural alteration in the G4 DNA structure from hybrid to unusual but more stable, parallel telomeric G4 DNA in the presence of K^+ ion, whereas the one with morpholine termini, **CBM**, was found to be inefficient in this regard. Thus, SAR established that the piperazine residues attached to the benzimidazole moiety were crucial toward the topological alteration in the G4 DNA structure. The high melting temperature of the parallel G4 DNA formed in the presence of each ligand reveals that the equilibrium between G4 structure and the single-stranded form is shifted significantly toward the higher order structures. The ligands **CMP** and **CHP** were also highly effective toward eliciting telomerase inhibition, and the IC_{50} below 1 μM indicates that these are among the best of the benzimidazole derivatives reported so far. Moreover, the carbazole based ligands were found to be remarkably superior to the first generation phenyl based benzimidazole ligands (Figure 1C, ligand **5**),[13a−d] as evident from both physical and biological experiments (Supporting Information, Figure S20). Manifestation of the selective cancer cell nuclear internalization and nuclear fragmentation, cytotoxicity at the low ligand concentration, and ability to induce cell death through an apoptotic pathway reveals their possible utility as an anticancer drug.

MATERIALS AND METHODS

Materials. All starting materials were from the best known commercial sources and used as received. All solvents were from Merck, and they were distilled and/or dried prior to use whenever necessary. All tested ligands were found to be at least >95% pure by elemental analysis.

Synthesis. *5-(4-Methylpiperazin-1-yl)-2-nitroaniline (**6a**).* 5-Chloro-2-nitroaniline (2 g, 11.6 mmol) was taken in dry DMF (5 mL), and to that, 4-methylpiperazine (1.4 g, 13.8 mmol) and anhydrous K_2CO_3 (2.5 g, 18 mmol) were added. The mixture was then heated at 110 °C for 12 h under a N_2 atmosphere until TLC showed the disappearance of 5-chloro-2-nitroaniline. The crude compound was suspended in water, and the product was extracted with ethyl acetate. The organic layer was washed twice with water, dried over anhydrous Na_2SO_4, and concentrated. This afforded a product which was adjudged as pure by TLC (1% MeOH/$CHCl_3$ on precoated silica gel) and isolated as a bright yellow solid (2.46 g, 90% yield).

^{1}H NMR ($CDCl_3$, 300 MHz): δ ppm 2.34 (s, 3H). 2.52 (t, J = 4.8, 4H), 3.37 (t, J = 4.8, 4H), 5.94 (s, 1H), 6.14 (bs), 6.30 (d, J = 9.3 Hz, 1H), 8.02 (d, J = 9.3 Hz, 1H); HRMS: m/z = 259.1271 $[M + Na]^+$; Calcd = 259.1273 $[M + Na]^+$; mp 154 °C (lit. 154 °C).[13a]

*2-[4-(3-Amino-4-nitro-phenyl)-piperazin-1-yl]-ethanol (**7a**).* 5-Chloro-2-nitroaniline (2 g, 11.6 mmol) was taken in dry DMF (5 mL), and 2-piperazin-1-yl-ethanol (3 g, 23.08 mmol) and K_2CO_3 (4.8 g, 34.6 mmol) were added to the solution. This mixture was then heated at 110 °C under a N_2 atmosphere for 12 h until TLC showed the disappearance of 5-chloro-2-nitroaniline. The crude compound was suspended in water, and the product was extracted with ethyl acetate. The organic layer was washed twice with water, dried over anhydrous Na_2SO_4, and concentrated. This afforded a pure product as confirmed by TLC (1% MeOH/$CHCl_3$ on precoated silica gel) and was isolated as a bright yellow solid (2.93 g, 95% yield).

^{1}H NMR (300 MHz, $CDCl_3$): δ ppm 2.59−2.65 (m, 6H), 3.4 (t, J = 4.8, 4H), 3.7 (t, J = 4.8, 2H), 5.95 (d, J = 2.7 Hz, 1H), 6.1 (bs, 2H, NH_2), 6.29 (dd, J = 9.3, J = 2.7, 1H), 8.02 (d, J = 9.3, 1H); HRMS: m/z = 267.1457 $[M + H]^+$; Calcd = 267.1457 $[M + H]^+$; mp 163 °C (lit. 163 °C).[13a]

*5-Morpholino-2-nitrobenzenamine (**8a**).* A mixture of 5-chloro-2-nitrobenzenamine (1 g, 1.8 mmol), morpholine (2 mL), and dry K_2CO_3 (1.2 g, 9 mmol) was taken along with 5 mL of dry DMF and heated at 110 °C under a nitrogen atmosphere for 12 h. The reaction mixture was then dried under a vacuum, and 50 mL of cold water was added to it to form a yellow colored precipitate which was filtered off and washed several times with distilled water and then dried, affording a yellow colored product which was adjudged to be pure by TLC (2% MeOH/$CHCl_3$ on precoated silica gel) (1.23 g, 95%).

^{1}H NMR (400 MHz, DMSO-d_6): δ ppm 7.82 (d, J = 10, 1H), 7.28 (s, 2H), 6.39 (dd, J = 9.8, J = 2.8, 1H), 6.2 (d, J = 2.8, 1H), 3.70 (t, J = 4.8, H), 3.27 (t, J = 4.8, 4H); IR (KBr): 3448, 3335, 3179, 3088, 2973, 2928, 2872, 2846, 1618, 1234, 1123, 892 cm^{-1}; HRMS: m/z = 246.0858 $[M + Na]^+$; Calcd = 246.0855 $[M + Na]^+$; mp 188 °C.

*4-(4-Methylpiperazin-1-yl)benzene-1,2-diamine (**6**).* Compound **6a** (206 mg) was taken along with 100 mg of Pd/C (10%) in ethanol and stirred under a H_2 atmosphere (1 atm pressure) for 12 h when the yellow solution turned colorless. The reaction mixture was then passed through a Celite bed under nitrogen flow and used for the next reaction without any further purification, as the diamine product was found to be highly unstable.

*2-(4-(3,4-Diaminophenyl)piperazin-1-yl)ethanol (**7**).* Compound **7** has been synthesized from **7a** following a similar procedure as described for compound **6**.

*4-Morpholinobenzene-1,2-diamine (**8**).* Compound **8** has been synthesized from **8a** following a similar procedure as described for compound **6**.

*9-(4-Bromobutyl)-9H-carbazole (**9**).* To a mixture of TBAI (277 mg, 0.75 mmol), carbazole (3 g, 18 mmol), and 11.67 g (54 mmol) of 1,4-dibromobutane in benzene, aqueous 50% NaOH solution (9 mL) was added at rt. The mixture was then stirred for 6 h at the same temperature and then poured into water and extracted with DCM. The organic layer was passed through a bed of dry Na_2SO_4 and evaporated to get a crude product which was purified by silica gel column chromatography with a hexane/ethyl acetate mixture as the eluent, yielding a white solid (5.4 g, 72%).

^{1}H NMR (400 MHz, $CDCl_3$): δ ppm 8.1 (d, J = 7.6, 2H), 7.47 (m, 4H), 7.24 (dd, J = 4.5, J = 7.8, 2H), 4.36 (t, J = 6.8, 2H), 3.38 (t, J = 6.8, 2H), 2.07 (m, 2H), 1.91 (m, 2H); HRMS: m/z = 302.0545 $[M + H]^+$; Calcd = 302.0544 $[M + H]^+$; mp 101 °C (lit. 100 °C).[37]

*9-(4-(4-Methylpiperazin-1-yl)butyl)-9H-carbazole (**10**).* Compound **9** (900 mg, 2.98 mmol), 596 mg (5.96 mmol) of *N*-methylpyperazine, and 823 mg of dry K_2CO_3 were stirred together in 30 mL of dry acetonitrile for 6 h. Then, the reaction mixture was dried and partitioned between water and chloroform. The organic layer was separated and passed through a bed of dry Na_2SO_4. The filtrate was collected and evaporated to get an off-white sticky solid product which was adjudged to be pure by TLC (3% MeOH/$CHCl_3$ on precoated silica gel) (852 mg, 89%).

^{1}H NMR (300 MHz, $CDCl_3$): δ ppm 8.1 (d, J = 7.8, 2H), 7.44 (m, 4H), 7.23 (dd, J = 4.5, J = 7.8, 3H), 4.33 (t, J = 6.8, 2H), 2.35 (m, 10H), 2.27 (s, 3H), 1.91 (m, 2H), 1.58 (m, 2); HRMS: m/z = 322.2283 $[M + H]^+$; Calcd = 322.2283 $[M + H]^+$.

*9-(4-(4-Methylpiperazin-1-yl)butyl)-9H-carbazole-3,6-dicarbaldehyde (**11**).* Compound **10** (1 g, 3.12 mmol) and 850 mg (6.24 mmol) of anhydrous $ZnCl_2$ were taken together in a round-bottom flask (100 mL) along with 6 mL of dry DMF and heated at 100 °C for 15 min. This was followed by cooling to rt. To this, 2.9 mL (31.2 mmol) of $POCl_3$ was added dropwise upon cooling over an ice-bath for 15 min followed by heating at 100 °C for 24 h. Then, the reaction mixture was evaporated under a vacuum to remove the excess DMF and quenched carefully by addition of ice-cold water followed by neutralization with concentrated KOH solution. The mixture was finally extracted using ethyl acetate, and the organic layer was passed through a bed of dry Na_2SO_4. The filtrate was collected and evaporated to get a brown gummy mass which was purified by silica gel column chromatography using chloroform/methanol as the eluent. The final product came at 3% methanol/chloroform as a light yellow solid which was adjudged to

dx.doi.org/10.1021/jm500427n | J. Med. Chem. XXXX, XXX, XXX−XXX

be pure by TLC (5% MeOH/$CHCl_3$ on precoated silica gel) (881 mg, 75%).

^{1}H NMR (300 MHz, $CDCl_3$): δ ppm 10.14 (s, 2H), 8.67 (s, 2H), 8.09 (d, J = 8.7, 2H), 7.58 (d, J = 8.4, 2H), 4.43 (t, J = 6.9, 2H), 2.42−2.37 (m, 6H), 2.31 (s, 3H), 2.05−1.96 (m, 6H), 1.6 (m, 2H); IR (KBr): 3052, 2964, 2936, 2786, 2736, 1683, 1593, 1488, 1385, 1345, 1285, 1202, 1126, 1014, 812 cm^{-1}. HRMS: m/z = 378.2183; Calcd = 378.2182 $[M + H]^+$; mp 218 °C; Anal. (calcd for $C_{23}H_{27}N_3O_2$): C, 73.18; H, 7.21; N, 11.13; found: C, 73.82; H, 7.13; N, 11.21.

*3-(5-(4-Methylpiperazin-1-yl)-1H-benzo[d]imidazol-2-yl)-6-(6-(4-methylpiperazin-1-yl)-1H-benzo [d]imidazol-2-yl)-9-(4-(4-methylpiperazin-1-yl)butyl)-9H-carbazole (**1, CMP**).* Freshly prepared compound **6** (180 mg, 0.87 mmol) was taken with 164 mg (0.44 mmol) of compound **11** in 30 mL of ethanol. To that, 87 mg (0.45 mmol) of $Na_2S_2O_5$ dissolved in 1 mL of water was added and refluxed for 12 h until the reactants were consumed as indicated from TLC. Then, the reaction mixture was cooled and filtered. The supernatant was evaporated and purified by repetitive precipitation from a methanol/ethyl acetate mixture, yielding a light brown powder (195 mg, 60%).

^{1}H NMR (400 MHz, CD_3OD): δ ppm 8.79 (s, 2H), 8.06 (d, J = 8, 2H), 7.5 (d, J = 8.4, 2H), 7.45 (d, J = 8.4, 2H), 7.12 (s, 2H), 7 (d, J = 8.8, 2H), 4.36 (s, 2H), 3.8 (s, 4H), 2.99 (s, 9H), 2.87 (s, 4H), 2.85 (s, 2H), 2.71 (s, 6H), 2.5 (s, 4H), 2.4 (m, 6H), 1.8(s, 2H), 1.48(s, 2H); ^{13}C NMR (CD_3OD): δ ppm 152.24, 148.31, 142.52, 137.89, 133.21, 125.47, 123.43, 120.09, 119.22, 116.14, 110.62, 101.81, 65.19, 57.50, 55, 54.03, 51.56, 44.32, 44.18, 27.13, 24.02, 15.48; IR (KBr): 3458, 2931, 2702, 1638, 1602, 1459, 1384, 1240, 1140, 1023, 963, 814 cm^{-1}; HRMS: m/z = 750.4717 $[M + H]^+$; Calcd = 750.4720 $[M + H]^+$; mp >280 °C; Anal. (calcd for $C_{45}H_{55}N_{11}\cdot 0.5H_2O$): C, 71.21; H, 7.44; N, 20.30; found: C, 71.42; H, 7.40; N, 20.27.

*3-(5-(4,2-Hydroxyethylpiperazin-1-yl)-1H-benzo[d]imidazol-2-yl)-6-(6-(4-methylpiperazin-1-yl)-1H-benzo[d]imidazol-2-yl)-9-(4-(4-methylpiperazin-1-yl)butyl)-9H-carbazole (**2, CHP**).* Compound **2** was synthesized following a similar procedure as described for **1**. Yield = 60%.

^{1}H NMR (400 MHz, CD_3OD): δ ppm 8.72 (s, 2H), 7.91 (d, J = 8.4, 2H), 7.36 (m, 4H), 6.98 (s, 2H), 6.85 (d, J = 8.4, 2H), 4.2 (s, 2H), 3.69 (t, J = 5.6, 4H), 2.81 (s, 8H), 2.7 (t, J = 5.2, 8H), 2.6 (d, J = 2, 4H), 2.53 (s, 4H), 2.42 (s, 4H), 2.29 (m, 6H), 1.73 (s, 2H), 1.44 (s, 2H); ^{13}C NMR (CD_3OD): δ ppm 153.39, 149.07, 142.77, 139.35, 135.24, 125.82, 124.07, 121.46, 120.20, 116.48, 115.82, 110.69, 101.83, 65.04, 60.81, 58.89, 57.99, 54.78, 54.34, 52.35, 50.67, 44.96, 27.41, 24.50, 22.79, 15.44; IR (KBr): 3440, 2943, 2823, 1633, 1603, 1451, 1403, 1239, 1188, 1138, 1020, 966, 814 cm^{-1}; HRMS: m/z = 810.4930 $[M + H]^+$; Calcd = 810.4931 $[M + H]^+$; mp >250 °C; Anal. (calcd for $C_{47}H_{59}N_{11}O_2$): C, 69.69; H, 7.34; N, 19.02; found: C, 69.42; H, 7.40; N, 19.08.

*9-(4-(4-Methylpiperazin-1-yl)butyl)-3,6-bis(6-morpholino-1H-benzo[d]imidazol-2-yl)-9H-carbazole (**3, CBM**).* The freshly prepared diamine **8** (205 mg, 1.1 mmol) was mixed with the dialdehyde **11** (200 mg, 0.53 mmol) in 50 mL of ethanol, and to that, an aqueous solution of 110 mg of $Na_2S_2O_5$ was added and the mixture was refluxed for 12 h. The reaction mixture was then cooled and filtered. The filtrate was evaporated to dryness which afforded a crude yellow mass which was dissolved in 5 mL of methanol and precipitated with the addition of ethyl acetate. The precipitation process was repeated twice to get a yellowish product which was adjudged to be pure by TLC (10% MeOH/$CHCl_3$ on precoated silica gel) (325 mg, 85%).

^{1}H NMR (400 MHz, DMSO-d_6): δ ppm 12.67 (br, 2H), 9.06 (s, 2H), 8.31 (d, J = 8.8, 2H), 7.82 (d, J = 8.8, 2H), 7.48 (d, J = 8, 2H), 7.05 (s, 2H), 6.95 (d, J = 8, 2H), 4.5 (s, 2H), 3.76 (s, 8H), 3.1 (s, 4H), 2.7−2.34 (m, 10H), 1.82 (s, 2H), 1.52 (s, 2H); ^{13}C NMR (DMSO-d_6): δ ppm =154.12, 151.77, 148.20, 147.78, 141.27, 127.31, 124.70, 123.79, 122.52, 122.38, 122.02, 118.54, 113.27, 110.25, 105.49, 98.93, 66.41, 61.44, 59.82, 56.30, 53.09, 50.48, 43.75, 26.27, 23.07, 15.22; IR (KBr): 2955, 2856, 2822, 2690, 1633, 1604, 1449, 1402, 1378, 1352, 1299, 1240, 1186, 1138, 1115, 980, 965, 900, 812 cm^{-1}; HRMS: m/z = 724.4086; Calcd = 724.4087 $[M + H]^+$; mp >300 °C; Anal. (calcd for $C_{43}H_{49}N_9O_2$): C, 71.34; H, 6.82; N, 17.4; found: C, 71.82; H, 6.76; N, 17.28.

*3,6-Bis(5-(5-(4-methylpiperazin-1-yl)-1H-benzo[d]imidazol-2-yl)-1H-benzo[d]imidazol-2-yl)-9-(4-(4-methylpiperazin-1-yl)butyl)-9H-carbazole (**4, CBhoe**).* The N-substituted carbazole-3,6-dicarbaldehyde **11** (50 mg, 0.133 mmol) was taken with 86 mg (0.266 mmol) of freshly prepared diamine (**17**) in 20 mL of ethanol and heated at 80 °C. An aqueous solution of $Na_2S_2O_5$ (30 mg) was added to the reaction mixture and refluxed with stirring for 12 h. The reaction mixture was then cooled, filtered, and dried under reduced pressure. The crude solid material was dissolved in methanol and repeatedly precipitated by adding ethyl acetate. The product was then further purified with preparative thin layer chromatography with a 1:1 methanol/chloroform mixture.

^{1}H NMR (400 MHz, DMSO-d_6): δ ppm 9.21 (s, 2H), 8.42 (d, J = 8.8, 2H), 8.37 (s, 2H), 8.04 (d, J = 8.8), 7.88 (d, J = 8.8, 2H), 7.73 (d, J = 8.4, 2H), 7.46 (d, J = 7.2, 2H), 7.03 (s, 2H), 6.94 (dd, J = 1.6, J = 8.6, 2H), 4.54 (s, 2H), 3.17−3.13 (m, 10H), 2.30−2.25 (m, 18H), 2.12 (s, 6H), 1.87 (s, 2H), 1.69 (s, 2H), 1.51 (s, 2H); ^{13}C NMR (DMSO-d_6): δ ppm 162.39, 154.97, 141.60, 128.05, 125.47, 122.45, 121.41, 119.13, 110.34, 79.09, 56.98, 54.84, 54.71, 52.51, 49.95, 48.57, 45.73, 45.69, 35.78, 30.78, 26.28, 23.48; mp >300 °C; IR (KBr): 3455, 2930, 2817, 2706, 1638, 1622, 1604, 1463, 1381, 1373, 1241, 1143, 1119, 1013, 961, 817, 806 cm^{-1}; HRMS: m/z = 982.5469; Calcd = 982.5469 $[M + H]^+$; Anal. (calcd for $C_{59}H_{63}N_{15}$): C, 72.15; H, 6.46; N, 21.39; found: C, 71.98; H, 6.41; N, 21.48.

Oligonucleotides. HPLC purified oligodeoxyribonucleotide (ODN) d[$G_3(T_2AG_3)_3$], abbreviated as Hum_{21}, was purchased from Sigma Genosys, Bangalore. Their purity was confirmed using high resolution sequencing gel. The molar concentration of each ODN was determined from absorbance measurements at 260 nm based on its molar extinction coefficients (ε_{260}) of 215 000 for d[$G_3(T_2AG_3)_3$].

G4 DNA Formation. Hum_{21} [5′-$G_3(T_2AG_3)_3$-3′] sequence was incubated in a buffer containing 10 mM Tris−HCl (pH 7.4), 0.1 mM EDTA, and 0.1 M of indicated salt and heated at 95 °C for 5 min and cooled slowly to 24 °C over 24 h. The formation of G4 DNA has been confirmed by circular dichroic spectral signature with that reported in the literature[13c−e] as well as by PAGE.

Circular Dichroism Spectroscopy. The CD experiments were performed in a Jasco J-815 CD spectropolarimeter equipped with a Peltier temperature controller in 1 cm quartz cuvette at 20 °C. To the preformed G4 (4 μM) in 10 mM Tris−HCl (pH 7.4), 0.1 M either NaCl or KCl, and 0.1 mM EDTA, aliquots of ligand solutions (prepared in the corresponding buffer) were added and incubated for 15 min prior to recording with a scan rate of 50 nm/min.

DNA Melting Experiment. The melting experiments were performed in a Jasco J-815 CD spectropolarimeter equipped with a Peltier temperature controller. DNA and DNA−ligand complexes were placed in a 1 cm quartz cuvette, charged in the temperature range from 20 to 90 °C, and monitored with an increase in the temperature range of 0.5 °C/min. All the experiments were repeated twice, and an average value has been reported with an error of ±0.5 °C. The data were plotted with Origin 8.0 software and the CD signal intensities were normalized to the range between 1 and 0.[13,38] The ligand solutions of 10 mM have been prepared in Milli-Q water/biological grade DMSO and diluted in the corresponding buffer related to the experiment.

Fluorescence Spectroscopy. Fluorescence emission spectra were recorded on a Carey Eclipse Varian spectrophotometer using quartz cells with a path length of 1 cm. The temperature of the sample component was maintained at 20 °C using a Peltier controller. To 0.4 μM of the ligand in specified buffer, 4 μL of 10 μM preformed G4 DNA of the corresponding buffer was added and incubated for 10 min prior to recording. The ligand solutions were excited at 300 nm (for **CMP**, **CHP**, and **CBM**) or 330 nm (for **CBhoe**) with a slit width of 10/10 nm. The data have been processed using Origin 8.0 software.

G4-FID Assays. A solution of 1 μM TO in Tris−HCl (pH 7.4) buffer containing 0.1 M KCl and 0.1 mM EDTA was taken in a 500 μL cell. The displacement assays were performed by adding increasing ligand concentration to the preformed DNA−TO complex (1 μM TO + 0.5 μM G4 DNA; 1 μM TO + 0.33 μM CT DNA; 1 μM TO + 0.33 μM Telo ds DNA) followed by measuring the emission spectra upon

dx.doi.org/10.1021/jm500427n | J. Med. Chem. XXXX, XXX, XXX−XXX

incubation for 5 min. The percentage of TO displacement is calculated from the fluorescence intensity (at λ = 531 nm, λ_{ex} = 501 nm) using the following equation: percentage of displacement = 100 − [(F_t/F_0) × 100], where F_t is the fluorescence intensity at each titration point and F_0 is the fluorescence of TO bound to DNA without any added ligand as described earlier.[20] The DC_{50} values have been calculated from the plot of the percentage of fluorescence intercalator displacement vs added ligand concentration.

S1 Nuclease Assay. S1 nuclease assay was performed as described in the reported protocol.[39] The 5′-end of Hum_{21} DNA was labeled with ^{32}P-ATP and purified using gel electrophoresis. The radioactively labeled DNA was then mixed with cold DNA and annealed in the presence of KCl to form the G4 DNA structure. The G4 DNA was incubated with the indicated ligand for 4 h before performing the S1 nuclease assay. A sample of 2 μM (cold + labeled) of 25 μL of DNA (ss- or G4-) was treated with 20 U of S1 nuclease in 1X S1 nuclease buffer for 2 min, and the reaction was quenched by the addition of 100 μL of stop buffer (0.3 M sodium acetate, 0.25 μg/mL CT DNA, 0.1 mM EDTA) followed by ethanol precipitation and washing with 70% ethanol. The reaction products were then vacuum-dried and resuspended in formamide dye and loaded on a 15% polyacrylamide urea sequencing gel along with a reference A+G ladder.

The reference A+G ladder was prepared following a reported protocol.[40] The 5′-end labeled Hum_{21} DNA (10 μL) was incubated with 25 μL of 100% formic acid at 25 °C for 5 min and terminated with 200 μL of hydrazine stop buffer (0.3 M sodium acetate, 250 μg/mL CT DNA, 0.1 mM EDTA) followed by ethanol precipitation. The product was vacuum-dried and treated with 10% of 70 μL of piperidine at 90 °C for 30 min. It was dried under a vacuum centrifuge, excess piperidine was removed by evaporating the sample twice from water, and it was resuspended in formamide dye before loading on a 15% polyacrylamide urea sequencing gel for 90 min against a voltage of 1800 V. Gel was transferred to a Whatman (3 mm) paper, dried, and exposed to a phosphor imaging screen, and the resulting image was captured using a Fuji-5000 phosphorimager.

Cell Viability Assay. The cells were seeded in 96-well plates (15.0 × 10^3/well). Cells were grown for 72 h before treatment to obtain >70% confluency and exposed to either various concentrations of ligands or an equivalent volume of DMSO (0.1%) in the presence of 10% FBS. After 72 h of incubation at 37 °C in a humidified atmosphere of 5% CO_2, the old medium was replaced with the fresh medium containing 10% FBS in DMEM and cells were further grown post treatment. Then, 20 μL of 5 mg/mL methyl thiazolyl tetrazolium (MTT) reagent was added to 200 μL of the medium present in each well and cells were further incubated for 4 h. The old medium was discarded, formazan crystals were dissolved in DMSO, and a reading (fluorescence emission intensity, FI) was taken at 595 nm in the ELISA plate reader. All ligand doses were parallel tested in triplicate. The percentage of cell viability was calculated using the following formula: % cell viability = [($FI_{(595)}$ of treated cells − $FI_{(595)}$ of plain DMSO)/($FI_{(595)}$ of untreated cells − $FI_{(595)}$ of plain DMSO)] × 100.

Long-Term Cell Viability Assay. In a typical long-term viability assay protocol, cells were grown in 6-well tissue culture plates at 5.0 × 10^4 per well and exposed to a sub-cytotoxic concentration of 2 μM or an equivalent volume of 0.1% DMSO. The cells in the control and ligand-exposed wells were counted, and wells were reseeded with a half population of cells. This process was continued for 15 days. Cell population versus time (days) graphs were generated.

Annexin V-FITC and PI Staining Assay.[32] The Annexin V-FITC Apoptosis Detection kit (Sigma) was used to detect apoptosis induced by the ligands in HeLa cells after 12 h of incubation. In a typical experiment, cells were seeded at a density of 0.25 million in 6-well cell culture plates. After 24 h, cells were incubated with the ligands for 12 h at a final concentration of 10 μM. At the end, cells were washed properly with DPBS buffer followed by trypsinization and resuspended in 1X binding buffer (HEPES buffer containing 0.14 M NaCl and 2.5 mM $CaCl_2$). Thereafter, Annexin V-FITC conjugate was added to each of the cell suspensions and incubation was carried out for 10 min at room temperature while protecting from light. Then, each cell suspension was incubated with propidium iodide (PI) solution at a final concentration of 1 μg/mL for 5 min. Samples were then analyzed using an FACS Calibur flow cytometer (Becton-Dickinson). Apoptotic cells were shown to be stained only with Annexin V-FITC conjugate. Data obtained from the flow cytometry were analyzed using WinMDI software by considering a gated cell population for the detection of % apoptotic cells.

Confocal Microscopy. To visualize the intracellular internalization of ligands and apoptotic nuclei, confocal microscopic studies were undertaken. In a typical experiment, cells were cultured on glass coverslips placed in 12-well cell culture plates. Cells were treated with ligands (12 h, internalization; 24 h, apoptosis) followed by proper washing with DPBS buffer three times and fixed in 4% paraformaldehyde solution for 10 min. Cells were then rinsed again with DPBS buffer three times and treated with 0.1% Triton-X-100 for 5 min to permeabilize the cell membrane. After a proper wash again with DPBS buffer, the glass coverslips were taken out and treated with propidium iodide (PI) for nuclear counterstaining. Finally, after a repeated wash with DPBS buffer and autoclaved Milli-Q to control overstaining, the coverslips were mounted on glass slides and viewed under a confocal fluorescence microscope (Leica confocal microscope, SP5).

■ ASSOCIATED CONTENT

Ⓢ Supporting Information

Synthesis of compounds **11**−**16**, characterization of the key compounds, additional UV−vis titration, fluorescence, CD spectroscopic data, telomerase inhibition data, cytotoxicity data, and computational results. This material is available free of charge via the Internet at http://pubs.acs.org.

■ AUTHOR INFORMATION

Corresponding Author

*E-mail: sb@orgchem.iisc.ernet.in. Phone: (91)-80-2293 2664. Fax: (91)-80-2293 0529.

Notes

The authors declare no competing financial interest.

■ ACKNOWLEDGMENTS

This work was supported by J. C. Bose Fellowship, DST, to S.B. B.M. acknowledges CSIR for a senior research fellowship. The human foreskin fibroblast (HFF) cells were a kind gift from the Manipal University, Manipal.

■ ABBREVIATIONS USED

G4 DNA, G-quadruplex DNA; ODNs, oligodeoxynucleotides; CD, circular dichorism; ICD, induced circular dichorism; TRAP, telomerase repeat amplification protocol; FI, fluorescence intensity; THF, tetrahydrofuran; DMF, dimethylformamide; TBAI, tetrabutyl ammonium iodide; EDTA, ethylenediaminetetraacetic acid; MTT, methyl thiazolyl tetrazolium; PI, propidium iodide; DMSO, dimethyl sulfoxide; NMR, nuclear magnetic resonance; IR, infrared

■ REFERENCES

(1) Makarov, V. L.; Hirose, Y.; Langmore, J. P. Long G tails at both ends of human chromosomes suggest a C strand degradation mechanism for telomere shortening. *Cell* **1997**, *88*, 657−666.

(2) (a) Ducray, C.; Pommier, J. P.; Martins, L.; Boussin, F. D.; Sabatier, L. Telomere dynamics, end-to-end fusions and telomerase activation during the human fibroblast immortalization process. *Oncogene* **1999**, *18*, 4211−4223. (b) Harley, C. B.; Futcher, A. B.; Greider, C. W. Telomeres shorten during ageing of human fibroblasts. *Nature* **1990**, *345*, 458−460.

(3) Blackburn, E. H. Structure and function of telomeres. *Nature* **1991**, *350*, 569−573.

(4) Cortez-Gonzalez, X.; Zanetti, M. Telomerase immunity from bench to bedside: round one. *J. Transl. Med.* **2007**, *5*, 12−28.
(5) (a) Haider, S. M.; Parkinson, G. N.; Neidle, S. Crystal structure of the potassium form of an Oxytricha nova G-quadruplex. *J. Mol. Biol.* **2002**, *320*, 189−200. (b) Gowan, S. M.; Harrison, J. R.; Patterson, L.; Valneti, M.; Read, M. A.; Neidle, S.; Kelland, L. R. A G-quadruplex-interactive potent small-molecule inhibitor of telomerase exhibiting *in vitro* and *in vivo* antitumor activity. *Mol. Pharmacol.* **2002**, *61*, 1154−1162.
(6) Maji, B.; Bhattacharya, S. Advances in the molecular design of potential anticancer agents via targeting of human telomeric DNA. *Chem. Commun.* **2014**, *50*, 6422−6438.
(7) Kim, M.-Y.; Gleason-Guzman, M.; Izbicka, E.; Nishioka, D.; Hurley, L. H. The different biological effects of telomestatin and TMPyP4 can be attributed to their selectivity for interaction with intramolecular or intermolecular G-quadruplex structures. *Cancer Res.* **2003**, *63*, 3247−3256.
(8) Burger, A. M.; Dai, F.; Schultes, C. M.; Reszka, A. P.; Moore, M. J.; Double, J. A.; Neidle, S. The G-quadruplex-interactive molecule BRACO-19 inhibits tumor growth, consistent with telomere targeting and interference with telomerase function. *Cancer Res.* **2005**, *65*, 1489−1496.
(9) Gunaratnam, M.; de la Fuente, M.; Hampel, S. M.; Todd, A. K.; Reszka, A. P.; Schätzlein, A.; Neidle, S. Targeting pancreatic cancer with a G-quadruplex ligand. *Bioorg. Med. Chem.* **2011**, *19*, 7151−7157.
(10) Bhattacharya, S.; Chaudhuri, P. Medical implications of benzimidazole derivatives as drugs designed for targeting DNA and DNA associated processes. *Curr. Med. Chem.* **2008**, *15*, 1762−1777.
(11) (a) Neidle, S.; Mann, J.; Rayner, E. L.; Baron, A.; Opoku-Boahen, Y.; Simpson, I. J.; Smith, N. J.; Fox, K. R.; Hartleyd, J. A.; Kellande, L. R. Symmetric bis-benzimidazoles: new sequence-selective DNA-binding molecules. *Chem. Commun.* **1999**, 929−930. (b) Chaudhauri, P.; Ganguly, B.; Bhattacharya, S. An experimental and computational analysis on the differential role of the potential isomers of symmetric bis-2-(pyridyl)-1*H*-benzimidazoles as DNA binding agents. *J. Org. Chem.* **2007**, *72*, 1912−1923.
(12) Li, G.; Huang, J.; Zhang, M.; Zhou, Y.; Zhang, D.; Wu, Z.; Wang, S.; Weng, X.; Zhou, X.; Yang, G. Bis(benzimidazole)pyridine derivative as a new class of G-quadruplex inducing and stabilizing ligand. *Chem. Commun.* **2008**, *38*, 4564−4566.
(13) (a) Jain, A. K.; Reddy, V. V.; Paul, A.; Muniyappa, K.; Bhattacharya, S. Synthesis and evaluation of a novel class of G-quadruplex-stabilizing small molecules based on the 1,3-phenylene-bis(piperazinyl benzimidazole) system. *Biochemistry* **2009**, *48*, 10693−10704. (b) Bhattacharya, S.; Chaudhuri, P.; Jain, A. K.; Paul, A. Symmetrical bisbenzimidazoles with benzenediyl Spacer: The role of the shape of the ligand on the stabilization and structural alterations in telomeric G-quadruplex DNA and telomerase inhibition. *Bioconjugate Chem.* **2010**, *21*, 1148−1159. (c) Jain, A. K.; Paul, A.; Maji, B.; Muniyappa, K.; Bhattacharya, S. Dimeric 1,3-Phenylene-bis-(piperazinyl benzimidazole)s: Synthesis and structure-activity investigation on their binding with human telomeric G-quadruplex DNA and telomerase inhibition properties. *J. Med. Chem.* **2012**, *55*, 2981−2993. (d) Paul, A.; Jain, A. K.; Misra, S. K.; Maji, B.; Muniyappa, K.; Bhattacharya, S. Binding of gemini bisbenzimidazole drugs with human telomeric G-quadruplex dimers: effect of the spacer in the design of potent telomerase inhibitors. *PLoS One* **2012**, *7*, e39467. (e) Paul, A.; Maji, B.; Misra, S. K.; Jain, A. K.; Muniyappa, K.; Bhattacharya, S. Stabilization and structural alteration of the G-quadruplex DNA made from the human telomeric repeat mediated by Tröger's Base based novel benzimidazole derivatives. *J. Med. Chem.* **2012**, *55*, 7460−7471. (f) Maji, B.; Bhattacharya, S. Molecular design of synthetic benzimidazoles for the switchover of the duplex to G-quadruplex DNA recognition. *Chimia* **2013**, *67*, 39−43.
(14) Patrick, D. A.; Boykin, D. W.; Wilson, W. D.; Tanious, F. A.; Spychala, J.; Bender, B. C.; Hall, J. E.; Dykstra, C. C.; Ohemeng, K. A.; Tidwell, R. R. Anti-Pneumocystis carinii pneumonia activity of dicationic carbazoles. *Eur. J. Med. Chem.* **1997**, *32*, 78l−793.
(15) (a) Zhang, X.-F.; Zhang, H.-J.; Xiang, J.-F.; Li, Q.; Yang, Q.-F.; Shang, Q.; Zhang, Y.-X.; Tang, Y.-L. The binding modes of carbazole derivatives with telomere G-quadruplex. *J. Mol. Struct.* **2010**, *982*, 133−138. (b) Huang, F. C.; Chang, C. C.; Lou, P. J.; Kuo, I. C.; Chien, C. W.; Chen, C. T.; Shieh, F. Y.; Chang, T. C.; Lin, J. J. G-quadruplex stabilizer 3,6-bis(1-methyl-4-vinylpyridinium)carbazole diiodide induces accelerated senescence and inhibits tumorigenic properties in cancer cells. *Mol. Cancer Res.* **2008**, *6*, 955−964.
(16) Tanious, F. A.; Ding, D.; Patrick, D. A.; Tidwell, R. R.; Wilson, W. D. A new type of DNA minor-groove complex: carbazole dication-DNA interactions. *Biochemistry* **1997**, *36*, 15315−15325.
(17) Jin, B.; Zhang, X.; Zheng, W.; Liu, X.; Qi, C.; Wang, F.; Shangguan, D. Fluorescence light-up probe for parallel g-quadruplexes. *Anal. Chem.* **2014**, *86*, 943−52.
(18) Parkinson, G. N.; Lee, M. P. H.; Neidle, S. Crystal structure of parallel quadruplexes from human telomeric DNA. *Nature* **2002**, *417*, 876−880.
(19) (a) Campbell, N. H.; Parkinson, G. N.; Reszka, A. P.; Neidle, S. Structural basis of DNA quadruplex recognition by an acridine drug. *J. Am. Chem. Soc.* **2008**, *130*, 6722−6724. (b) Ranjan, N.; Davis, E.; Xue, L.; Arya, D. P. Dual recognition of the human telomeric G-quadruplex by a neomycin-anthraquinone conjugate. *Chem. Commun.* **2013**, *49*, 5796−5798.
(20) Monchaud, D.; Allain, C.; Bertrand, H.; Smargiasso, N.; Rosu, F.; Gabelica, V.; De Cian, A.; Mergny, J. L.; Teulade-Fichou, M. P. Ligands playing musical chairs with G-quadruplex DNA: a rapid and simple displacement assay for identifying selective G-quadruplex binders. *Biochimie* **2008**, *90*, 1207−1223.
(21) Ambrus, A.; Chen, D.; Dai, J.; Bialis, T.; Jones, R. A.; Yang, D. Human telomeric sequence forms a hybrid-type intramolecular G-quadruplex structure with mixed parallel/antiparallel strands in potassium solution. *Nucleic Acids Res.* **2006**, *34*, 2723−2735.
(22) Wang, Y.; Patel, D. J. Solution structure of the human telomeric repeat $d[AG_3(T_2AG_3)_3]$ G-tetraplex. *Structure* **1993**, *1*, 263−282.
(23) Xue, Y.; Kan, Z.; Wang, Q.; Yao, Y.; Liu, J.; Hao, Y.; Tan, Z. Human telomeric DNA forms parallel-stranded intramolecular G-quadruplex in K^+ solution under molecular crowding condition. *J. Am. Chem. Soc.* **2007**, *129*, 11185−11191.
(24) Li, J.; Correia, J. J.; Wang, L.; Trent, J. O.; Chaires, J. B. Not so crystal clear: the structure of the human telomere G-quadruplex in solution differs from that present in a crystal. *Nucleic Acids Res.* **2005**, *33*, 4649−4659.
(25) Bianco, S.; Musetti, C.; Krapcho, A. P.; Palumbo, M.; Sissi, C. Ni^{2+} and Cu^{2+} complexes of a phenanthroline-based ligand bind to G-quadruplexes at non-overlapping sites. *Chem. Commun.* **2013**, *49*, 8057−8059.
(26) Maji, B.; Samanta, S. K.; Bhattacharya, S. Role of pH controlled DNA secondary structures in the reversible dispersion/precipitation and separation of metallic and semiconducting single-walled carbon nanotubes. *Nanoscale* **2014**, *6*, 3721−3730.
(27) Sun, D. In vitro footprinting of promoter regions within supercoiled plasmid DNA. *Methods Mol. Biol.* **2010**, *613*, 223−233.
(28) (a) Reed, J.; Gunaratnam, M.; Beltran, M.; Reszka, A. P.; Vilar, R.; Neidle, S. TRAP−LIG, a modified telomere repeat amplification protocol assay to quantitate telomerase inhibition by small molecules. *Anal. Biochem.* **2008**, *380*, 99−105. (b) De Cian, A.; Cristofari, G.; Reichenbach, P.; De Lemos, E.; Monchaud, D.; Teulade-Fichou, M. P.; Shin-Ya, K.; Lacroix, L.; Lingner, J.; Mergny, J. L. Reevaluation of telomerase inhibition by quadruplex ligands and their mechanisms of action. *Proc. Natl. Acad. Sci. U. S. A.* **2007**, *104*, 17347−17352.
(29) Naasani, I.; Oh-Hashi, F.; Oh-Hara, T.; Feng, W. Y.; Johnston, J.; Chan, K.; Tsuruo, T. Blocking telomerase by dietary polyphenols is a major mechanism for limiting the growth of human cancer cells in vitro and in vivo. *Cancer Res.* **2003**, *63*, 824−830.
(30) Mergny, J. L.; Riou, J. F.; Mailliet, P.; Teulade-Fichou, M. P.; Gilson, E. Natural and pharmacological regulation of telomerase. *Nucleic Acids Res.* **2002**, *30*, 839−865.
(31) Sharma, H. W.; Sokoloski, J. A.; Perez, J. R.; Maltese, J. Y.; Sartorelli, A. C.; Stein, C. A.; Nichols, G.; Khaled, Z.; Telang, N. T.;

Narayanan, R. Differentiation of immortal cells inhibits telomerase activity. *Proc. Natl. Acad. Sci. U. S. A.* **1995**, *92*, 12343−12346.
(32) Mahesh, K. J.; Idris, M. M.; Srinivas, G.; Vinay, K. P.; Meghah, V.; Kavitha, M.; Reddy, C. R.; Mainkar, P. S.; Pal, B.; Chandrasekar, S.; Nagesh, N. Phenyl 1,2,3-triazole-thymidine ligands stabilize G-quadruplex DNA, inhibit DNA synthesis and potentially reduce tumor cell proliferation over 3′-azido deoxythymidine. *PLoS One* **2013**, *8*, e70798.
(33) Frisch, M. J.; Trucks, G. W.; et al. *Gaussian 03*; Gaussian, Inc.: Wallingford, CT, 2004.
(34) Case, D. A.; Darden, T. A.; Cheatham, T. E., III; Simmerling, C. L.; Wang, J.; Duke, R. E.; Luo, R.; Merz, K. M.; Pearlman, D. A.; Crowley, M.; Walker, R. C.; Zhang, W.; Wang, B.; Hayik, S.; Roitberg, A.; Seabra, G.; Wong, K. F.; Paesani, F.; Wu, X.; Brozell, S.; Tsui, V.; Gohlke, H.; Yang, L.; Tan, C.; Mongan, J.; Hornak, V.; Cui, G.; Beroza, P.; Mathews, D. H.; Schafmeister, C.; Ross, W. S.; Kollman, P. A. *Amber 9*; University of California: San Francisco, CA, 2006.
(35) Ghosh, S.; Pignot-Paintrand, I.; Dumy, P.; Defrancq, E. Design and synthesis of novel hybrid metal complex−DNA conjugates: key building blocks for multimetallic linear DNA nanoarrays. *Org. Biomol. Chem.* **2009**, *7*, 2729−2737.
(36) (a) Biffi, G.; Tannahill, D.; McCafferty, J.; Balasubramanian, S. Quantitative visualization of DNA G-quadruplex structures in human cells. *Nat. Chem.* **2013**, *5*, 182−186. (b) Largy, E.; Granzhan, A.; Hamon, F.; Verga, D.; Teulade-Fichou, M. P. Visualizing the quadruplex: from fluorescent ligands to light-up probes. *Top. Curr. Chem.* **2013**, *330*, 111−177. (c) Siddiqui-Jain, A.; Hurley, L. H. Visualizing the quadruplex. *Nat. Chem.* **2013**, *5*, 153−155. (d) Biffi, G.; Di Antonio, M.; Tannahill, D.; Balasubramanian, S. Visualization and selective chemical targeting of RNA G-quadruplex structures in the cytoplasm of human cells. *Nat. Chem.* **2014**, *6*, 75−80.
(37) Taranekar, P.; Fulghum, T.; Patton, D.; Ponnapati, R.; Clyde, G.; Advincula, R. Investigating carbazole jacketed precursor dendrimers: sonochemical synthesis, characterization, and electrochemical crosslinking properties. *J. Am. Chem. Soc.* **2007**, *129*, 12537−12548.
(38) Tran, P. L.; Largy, E.; Hamon, F.; Teulade-Fichou, M. P.; Mergny, J. L. Fluorescence intercalator displacement assay for screening G4 ligands towards a variety of G-quadruplex structures. *Biochimie* **2011**, *93*, 1288−1296.
(39) Harada, F.; Dahlberg, J. E. Specific cleavage of tRNA by nuclease S1. *Nucleic Acids Res.* **1975**, *2*, 865−871.
(40) Maxam, A. M.; Gilbert, W. A new method for sequencing DNA. *Proc. Natl. Acad. Sci. U. S. A.* **1977**, *74*, 560−564.